target is suggested, but the optimum configuration cannot yet be specified; a pulsed rotating field[17] or a combination of dc and oscillating fields may be more effective than a simple rotating field.

ACKNOWLEDGMENTS

We wish to acknowledge with much thanks the help of Dr. T. J. Schmugge in the initial stages of this work; many helpful discussions with J. R. McColl on the the theory of spin refrigerators and computer programming; the able assistance of R. L. Ballard in computing the Yb polarization; and the calculation of the Yb:YES relaxation by Dr. G. H. Larson. This research has been supported in part by the U. S. Office of Naval Research and the U. S. Atomic Energy Commission; this paper is AEC document report code No. UCB-34P20-35.

PHYSICAL REVIEW VOLUME 152, NUMBER 1 2 DECEMBER 1966

Optical Absorption of Tetrahedral Fe^{2+} ($3d^6$) in Cubic ZnS, CdTe, and $MgAl_2O_4$

G. A. SLACK, F. S. HAM, AND R. M. CHRENKO
General Electric Research and Development Center, Schenectady, New York
(Received 17 June 1966)

The optical absorption spectrum of substitutional Fe^{2+} ions at concentrations from 2×10^{18} to 4×10^{20} cm^{-3} has been studied for cubic ZnS, CdTe, and $MgAl_2O_4$ single crystals from 3 to 300°K. The Fe^{2+} ions show a single broad absorption band at 300°K in the infrared region between 1500 and 7500 cm^{-1} (1.3 to 6.7 μ) that arises from the $^5E \rightarrow {}^5T_2$ transition. At low temperatures this band shows many distinct lines which are identified as resulting from zero-phonon and phonon-assisted transitions between the spin-orbit levels of ^5E and $^5T_2$ in tetrahedral symmetry. The levels of ^5E are found to be described well by crystal-field theory: There are five uniformly spaced levels split in second order by spin-orbit interactions, with an interval given by 15, 10, and 13 cm^{-1} for Fe^{2+} in ZnS, CdTe, and $MgAl_2O_4$, respectively. The levels of $^5T_2$ do not fit the predictions of crystal-field theory; they can, however, be understood if a moderately strong Jahn-Teller effect occurs in the $^5T_2$ state, so that the first-order spin-orbit splitting of $^5T_2$ is quenched to a small fraction of its crystal-field value. Values for this Jahn-Teller energy of 535, 255, and 945 cm^{-1} are derived from the data for ZnS, CdTe, and $MgAl_2O_4$, respectively. A phenomenological Hamiltonian is found which describes the dynamical Jahn-Teller effects in ZnS very well, and which may also be appropriate for $MgAl_2O_4$ but does not suffice for CdTe. An alternative interpretation of the spectrum for Fe^{2+} in ZnS, not requiring so strong a Jahn-Teller effect, more nearly accords with the predictions of crystal-field theory, but at the expense of assuming that some of the observed zero-phonon lines arise from Fe^{2+} associated with some other defect common to all samples, or from a mixture of cubic and hexagonal regions within the crystals. Values of the cubic-field parameter Dq for Fe^{2+} in these crystals are -340, -248, and -447 cm^{-1} for ZnS, CdTe, and $MgAl_2O_4$, respectively. The phonon-assisted transitions yield values for the transverse acoustic, longitudinal acoustic, transverse optic, and longitudinal optic phonons in ZnS and CdTe which are 115, 184, 296, 331 cm^{-1} and 65, 105, 140, 180 cm^{-1}, respectively.

I. INTRODUCTION

THE optical absorption spectra of ions of the first transition series in tetrahedral coordination in various crystalline solids have been studied in a number of investigations.[1–21] These spectra are of interest for comparison with the more familiar spectra of these ions in octahedral coordination, and as a test of the applicability of crystal-field theory to the tetrahedral case. The purpose of this paper is to report observations on the optical absorption spectra of tetrahedral Fe^{2+} in cubic ZnS, CdTe, and $MgAl_2O_4$ over the tem-

[1] W. W. Coblentz, Carnegie Instit. Wash. Publ. **97**, 1908, Part VI, p. 57.
[2] D. S. McClure, J. Phys. Chem. Solids **3**, 311 (1957).
[3] W. Low and M. Weger, Phys. Rev. **118**, 1119 (1960); **118**, 1130 (1960).
[4] R. Pappalardo, D. L. Wood, and R. C. Linares, Bull. Am. Phys. Soc. **5**, 516 (1960).
[5] R. E. Dietz and R. Pappalardo, Bull. Am. Phys. Soc. **5**, 416 (1960); **6**, 110 (1961).
[6] R. Pappalardo, J. Mol. Spectr. **6**, 554 (1961).
[7] R. Pappalardo and R. E. Dietz, Phys. Rev. **123**, 1188 (1961).
[8] R. Pappalardo, D. L. Wood, and R. C. Linares, J. Chem. Phys. **35**, 1460 (1961).
[9] R. Pappalardo, D. L. Wood, and R. C. Linares, J. Chem. Phys. **35**, 2041 (1961).
[10] H. A. Weakliem and D. S. McClure, J. Appl. Phys. **33**, 347S (1962).
[11] H. A. Weakliem, J. Chem. Phys. **36**, 2117 (1962).
[12] J. Ferguson, J. Chem. Phys. **39**, 116 (1963).
[13] J. W. Allen, Physica **29**, 764 (1963).
[14] R. E. Dietz, H. Kamimura, M. D. Sturge, and A. Yariv, Phys. Rev. **132**, 1559 (1963).
[15] D. S. McClure, J. Chem. Phys. **39**, 2850 (1963).
[16] R. Pappalardo, Spectrochim. Acta **19**, 2093 (1963).
[17] A. I. Ryskin, G. I. Khil'ko, B. I. Maksakov, and K. K. Dubenskii, Opt. i Spektroskopiya **16**, 274 (1962) [English transl.: Opt. Spectr. **16**, 149 (1964)].
[18] S. Ibuki and D. Langer, J. Phys. Soc. Japan **19**, 422 (1964).
[19] G. A. Slack, Phys. Rev. **134**, A1268 (1964).
[20] D. Langer and S. Ibuki, Phys. Rev. **138**, A809 (1965).
[21] I. Broser, H. Maier, and H. J. Schulz, Phys. Rev. **140**, A2135 (1965).

perature range 3 to 300°K, and to propose an interpretation of these spectra on the basis of crystal field theory[22] supplemented by the dynamical Jahn-Teller effect.[23,24]

The present optical study of the energy levels of the Fe^{2+} ions has been stimulated by previous measurements of the thermal conductivity of Fe^{2+}-doped crystals of CdTe [25] and $MgAl_2O_4$ [19] at low temperatures. The measurements indicated that there were resonant phonon-scattering processes taking place between the spin-orbit levels of the Fe^{2+} ground state. An optical investigation of these levels was therefore desirable to establish their energies and thereby to aid in the interpretation of the thermal-conductivity results.

Absorption spectra for Fe^{2+} ions at tetrahedral sites have been reported previously for ZnS,[1,3,5] CdS,[5,7] CdTe,[19] and (Mg-Fe)Al_2O_4 [19] at temperatures near 300°K, and for CdS and ZnS at 4.2 and 78°K by Pappalardo and Dietz.[5,7] The energy levels of the $3d^6$ configuration have been derived by Low and Weger[3] on the basis of crystal-field theory, taking account of spin-orbit corrections through second-order terms. The ground state in tetrahedral symmetry should be ^5E, and the optical transition of interest is $^5E \rightarrow {}^5T_2$, which occurs in the range ≈ 2000 cm^{-1} to ≈ 6000 cm^{-1} for Fe^{2+} in the crystals that have been studied. Tetrahedral Fe^{2+} is a particularly good case for a test of crystal-field theory, for without any of the complications arising from crystal fields of lower symmetry one has five spin-orbit levels of ^5E and six of $^5T_2$ which give resolvable fine structure in the low-temperature spectra. The separations of these levels are predicted by crystal-field theory to depend significantly on only two spin-orbit parameters λ and λ^2/Dq, in addition to the cubic field splitting $10Dq$. Perturbing effects of higher states of Fe^{2+} are small and can be ignored, since for such small values of Dq as those of interest here no other state of Fe^{2+} lies below $\approx 18\,000$ cm^{-1}. Moreover, in tetrahedral symmetry the odd-parity part of the crystal field causes some of the fine-structure components of $^5E \rightarrow {}^5T_2$ to be electric-dipole allowed. The transitions are thus quite strong and easily observed, and the relative intensities of the various fine-structure components of the zero-phonon spectrum are then given unambiguously by theory as a further test of the interpretation.

Tetrahedral Fe^{2+} is also a favorable case in which to look for dynamical Jahn-Teller effects, in particular the partial quenching of spin-orbit interaction and related effects discussed recently by Ham.[24] Both ^5E and $^5T_2$ have orbital degeneracy, and the states are therefore unstable with respect to appropriate distortions in accordance with the Jahn-Teller theorem. Whereas in octahedral coordination the ^5E state is expected to show a strong Jahn-Teller effect (in analogy to the well-known Jahn-Teller effects[26] in the ^2E state of octahedral Cu^{2+}, and in agreement with O'Brien's analysis[27] of the optical absorption spectrum of Fe^{2+} in MgO), for Fe^{2+} in tetrahedral coordination the effect may be more pronounced for $^5T_2$ than for ^5E. Provided that the spin-orbit interaction is not too large with respect to the Jahn-Teller energy, one might then hope to find a substantial reduction of the spin-orbit splitting of $^5T_2$ for tetrahedral Fe^{2+} and consequently a profound modification of the fine structure of the zero-phonon spectrum from that predicted by crystal-field theory.

We shall in fact show that the fine structure observed in the absorption spectrum of tetrahedral Fe^{2+} in ZnS, CdTe, and $MgAl_2O_4$ does not agree with that predicted on the basis of crystal-field theory alone. An interpretation which supplements crystal-field theory by the dynamical Jahn-Teller effect can, however, account for the general features of the experimental spectra for all three crystals. We propose therefore as an interpretation of these spectra that in tetrahedral coordination the Jahn-Teller coupling causes a substantial change in the level structure of the $^5T_2$ excited state of Fe^{2+} in these crystals. Jahn-Teller effects in the ^5E ground state turn out, however, to be weak, the levels of this state being given satisfactorily by crystal-field theory. A detailed quantitative analysis of the zero-phonon lines in the absorption spectrum of Fe^{2+} in ZnS will be shown to fit this model very successfully. Alternatively, an interpretation for Fe^{2+} in ZnS that accords more nearly with the predictions of crystal-field theory is possible only if certain of the observed zero-phonon lines are assumed to arise from Fe^{2+} ions situated in a crystal field different from that seen by the majority of the Fe^{2+}.

The low-temperature spectra show pronounced structure from phonon-assisted transitions, in addition to the fine structure of the zero-phonon spectrum. The phonon-assisted peaks can be exploited to provide values for the energies of the maxima in the effective density of states of the phonons interacting with the Fe^{2+} ion. In the case of ZnS, these values will be shown to agree quite well with the energies of critical points in the phonon spectrum of pure ZnS determined from analyses[28–34] of the single- and multiphonon peaks in

[22] J. S. Griffith, *The Theory of Transition Metal Ions* (Cambridge University Press, Cambridge, England, 1961).
[23] H. A. Jahn and E. Teller, Proc. Roy. Soc. (London) **A161**, 117 (1937).
[24] F. S. Ham, Phys. Rev. **138**, A1727 (1965).
[25] G. A. Slack and S. Galginaitis, Phys. Rev. **133**, A253 (1964).
[26] M. C. M. O'Brien, Proc. Roy. Soc. (London) **A281**, 323 (1964).
[27] M. C. M. O'Brien, Proc. Phys. Soc. (London) **86**, 847 (1965).
[28] L. Merten, Z. Naturforsch. **13a**, 662; **13a**, 1067 (1958).
[29] A. K. Rajagopal and R. Srinivasan, Z. Physik **158**, 471 (1960).
[30] T. Deutsch, in *Proceedings of the Fifth International Conference on Semiconductors, Exeter, 1962* (Institute of Physics and the Physical Society, London, 1962), p. 505.
[31] R. Marshall and S. S. Mitra, Phys. Rev. **134**, A1019 (1962).
[32] L. Couture-Mathieu and J. P. Mathieu, Compt. Rend. **236**, 371 (1963).
[33] F. Abeles and J. P. Mathieu, Ann. Phys. (Paris) **3**, 5 (1958).
[34] H. Kaplan and J. J. Sullivan, Phys. Rev. **130**, 120 (1963).

TABLE. I. Single-crystal samples used for optical-absorption measurements.

Material	Sample number	Source	a_0[a]	Fe conc.[b]	t[c]	Color in bulk	Concentrations of Other Impurities[b]
ZnS	R139	Franklin, New Jersey	5.413	2.6[d]	14.7	Light Yellow	Cd=90, Mn=5, Si=4, Cu=2, Co=0.4, Others <1
ZnS	R118	Picos de Europa, Santander, Spain	5.412	41	0.97	Yellow	Cd=10, Cu=2, Co<0.2 Others <0.2
ZnS	R114, R114A	Big Four Mine, Summit County, Colorado	5.411	49	0.84	Yellow	Cd=110, Cu=0.6, Co<0.2, Others <0.2
ZnS	R140	Shiraita, Echigo, Japan	5.411	350	···	Yellow-Brown	Cd=45, Mn=9, Co=3, Cu=1, Si=1, Others <0.5
CdTe	R121	Synthetic	6.481	17	52	Opaque	Si∼1, others <1
CdTe	RX	Synthetic	6.480	88	1.4	Opaque	Ca∼1, Mg∼1, Si∼5, Others <1
$MgAl_2O_4$	R54	Burma	8.0868	9	15	Light Pink	Cr=20, V=30, Zn=30, Others <3[e]
$MgAl_2O_4$	R97	Ceylon	8.089	360	1.7	Bluish-Purple	Cr=35, Zn=20, Others <10[f]

[a] X-ray lattice parameter in Å, all of the crystals are cubic.
[b] The impurity concentrations have been determined by an emission spectrograph and are given in units of 10^{18} atoms/cm^3.
[c] t = sample thickness (in units of 10^{-2} cm) used for the low-temperature optical absorption curves.
[d] This is the Fe concentration determined from the optical absorption at 3500 cm^{-1} at 300°K. The sample contained many microscopically visible precipitate particles rich in Fe. The chemically determined total Fe concentration was 6.5 times greater than that given in the Table.
[e] See. G. A. Slack, Phys. Rev. **126**, 427 (1962).
[f] See Ref. 19.

the reststrahl region. The phonon spectra of CdTe and $MgAl_2O_4$ are not so well known, but we shall show that there is again reasonable agreement between our values and the available data[35–38] for the host crystals.

Recently, O'Brien[27] has discussed the effect of Jahn-Teller coupling on the optical absorption spectrum of Fe^{2+} in MgO. This case contrasts with ours in that for octahedral Fe^{2+} it is the ^5E state, rather than $^5T_2$, which shows the strong Jahn-Teller coupling. Moreover, we shall be primarily interested in what follows in the zero-phonon lines and in the effect of Jahn-Teller coupling in $^5T_2$ on the spin-orbit interaction. In the spectra considered by O'Brien, zero-phonon lines were evidently not resolved. O'Brien's concern, therefore, was to account for the splitting between the two broad peaks that fall well up into the phonon-assisted part of the spectrum. For these reasons, the theoretical treatment given below is quite different from that of O'Brien.

II. EXPERIMENTAL

A. Samples

The samples used in the present study were a combination of natural and synthetic single crystals. These are listed in Table I. The natural ZnS crystals were completely cubic ZnS, as nearly as could be told. [This point is covered in some detail in Sec. V under the subsection "Alternative Model."] The synthetic CdTe crystals were grown from the melt.[25] The iron concentrations listed in Table I were determined by wet chemical methods using solution colorimetry and are good to ±10%. All or almost all of the iron is in solid solution in these crystals. The crystals were examined by transmitted light with a microscope for possible precipitate phases, and only precipitate-free crystals were used. Crystal R139 of ZnS is an exception and is explained in Table I. An infrared image converter was used with the microscope for examining the CdTe. In ZnS and CdTe the Fe^{2+} substitutes[25,39] for the Zn^{2+} or Cd^{2+} in the lattice; in $MgAl_2O_4$ it substitutes[19] for the Mg^{2+}. The trace-metal impurities were determined by use of an emission spectrograph, and are good to within a factor of two. For the optical measurements, the samples were cut into the form of plates with plane-parallel faces with thicknesses from 1 to 0.005 cm, depending on the region of the spectrum being studied.

B. Experimental Technique

The optical-absorption measurements were made by using a combination of several different instruments. A Beckman IR7[40] grating instrument was used for the 800 to 4000 cm^{-1} range and a Beckman[40] DK-2A and Cary[41] Model 14 were used from 4000 cm^{-1} to 56 000 cm^{-1}. These instruments gave reliable results down to 5% and in some cases 1% sample transmission. The cryostat that was employed for controlling the sample

[35] R. E. Halsted, M. R. Lorenz, and B. Segall, J. Phys. Chem. Solids **22**, 109 (1961).
[36] P. Fisher and H. Y. Fan, Bull. Am. Phys. Soc. **4**, 409 (1959).
[37] A. Mitsuishi, H. Yoshinaga, and S. Fujita, J. Phys. Soc. Japan **13**, 1235 (1958); A. Mitsuishi, *ibid.* **16**, 533 (1961).
[38] V. V. Mitskevich, Fiz. Tverd. Tela **4**, 3035 (1962) [English transl.: Soviet Phys.—Solid State **4**, 2224 (1963)].
[39] G. Kullerud, Norsk Geol. Tidsskr. **32**, 61 (1953).
[40] Beckman Instruments Inc., Fullerton, California.
[41] Applied Physics Corporation, Monrovia, California.

temperature was of a simple design, similar to one used by Barrett.[42] The cryogenic liquids employed were liquid helium, hydrogen, and nitrogen.

The sample temperature was measured with a three-wire thermocouple. For the low-temperature region between 2 and 20°K a Au-Fe-versus-Cu pair of wires was used, while a Au-Co-versus-Cu pair was used from 20 to 300°K. The Au-Fe thermocouple has been studied by MacDonald *et al.*,[43] and by Berman, Brock, and Huntley.[44] The present wire was made by Sigmund Cohn[45] and contained 0.03 at.% of iron as judged[43] from its electrical resistivity. Its absolute thermoelectric power, S, was determined using both Pb and Ag +0.37 at.% Au as thermoelectric standards.[46] The absolute thermoelectric power of the Au-Co (1.8 at.% Co) and Cu have been reported previously.[46]

The optical-absorption coefficient, α, was computed from the experimental data taken at normal incidence at a particular photon energy using the expression

$$I=I_0(1-R)^2e^{-\alpha t}, \qquad (2.1)$$

where I is the intensity of the transmitted light, I_0 is the intensity of incident light, R is the reflectivity of a single surface at normal incidence, and t is the sample thickness. The reflection loss for a well polished optical surface can be computed from the index of refraction n if it is known. The data in the literature for n of ZnS for photon energies from 700 to 28 000 cm^{-1} is quite extensive,[47–54] and a composite of these data was used to determine R. The refractive index of CdTe from 4000 to 12 000 cm^{-1} has been measured by Marple,[55] and was used to compute R for the CdTe samples. The R values for $MgAl_2O_4$ were calculated from a combination[19] of n values and % R measurements over the phonon energy range from 800 to 48 000 cm^{-1}.

III. EXPERIMENTAL RESULTS

The results on the spectrum of Fe^{2+} in ZnS are the most complete of the three, and more data are available from the literature for ZnS than for either $MgAl_2O_4$ or CdTe. Hence the results for ZnS will be presented first, followed by CdTe and then $MgAl_2O_4$.

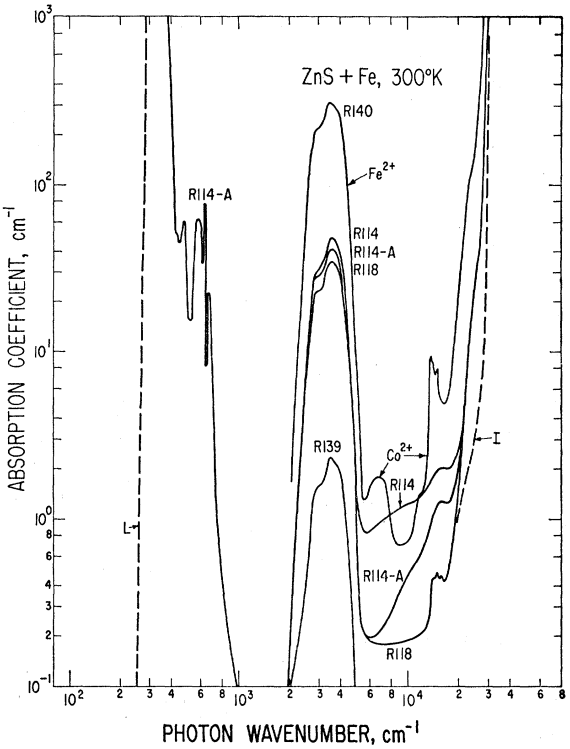

FIG. 1. The optical absorption coefficient α versus the photon wave number at 300°K for five different samples of natural, cubic ZnS with different Fe concentrations. The broad peak between 2000 and 5000 cm^{-1} is caused by Fe^{2+}. The peaks between 6000 and 18 000 cm^{-1} are caused by Co^{2+}. The multiphonon lattice bands between 400 and 1000 cm^{-1} can also be seen. The dashed L curve is the estimated low-energy cutoff of the reststrahl region, and the I curve is the intrinsic absorption edge of pure ZnS. The spectrometer resolution is 8 cm^{-1}.

A. Zinc Sulfide

The optical absorption coefficient, α, for five different samples of ZnS at 300°K, is shown in Fig. 1 as a function of photon wave number $\bar{\nu}$ (measured in cm^{-1}). The broad absorption band between 2000 and 5000 cm^{-1} is caused by the Fe^{2+} impurities, and in this part of the spectrum α is proportional to the iron concentration. This band was measured for all five ZnS samples studied. As can be seen from Table I, samples R114 and R114A were two nearly similar pieces of ZnS. The slight difference in α is caused by a slight variation in the iron content. Sample R118 has an almost identical α-versus-$\bar{\nu}$ curve in this region. The magnitude of α is somewhat less because of a slightly lower iron content (see Table I). Samples R140 and R139 show similar absorption curves, with both higher and lower α values. The absorption curve was used to determine the amount of Fe in solid solution in crystal R139 (see Table I).

[42] G. K. White, *Experimental Techniques in Low Temperature Physics* (Oxford University Press, London, 1959), p. 171.
[43] D. K. C. MacDonald, W. B. Pearson, and I. M. Templeton, Proc. Roy. Soc. (London) **266**, 161 (1962).
[44] R. Berman and D. J. Huntley, Cryogenics **3**, 70 (1963); R. Berman, J. C. F. Brock, and D. J. Huntley, *ibid.* **4**, 233 (1964).
[45] Sigmund Cohn Corporation, Mount Vernon, New York.
[46] G. A. Slack, Phys. Rev. **122**, 1451 (1961).
[47] E. T. Allen, J. L. Crenshaw, and H. E. Merwin, Am. J. Sci. **34**, 341 (1912).
[48] M. Mell, Z. Physik **16**, 244 (1923).
[49] A. Brun, Bull. Soc. Franc. Mineral **53**, 35 (1930).
[50] A. Cissarz, Z. Kristall. **82**, 438 (1932).
[51] J. R. DeVore, J. Opt. Soc. Am. **41**, 416 (1951).
[52] J. F. Hall and W. F. C. Ferguson, J. Opt. Soc. Am. **45**, 714 (1955).
[53] S. J. Czysak, W. M. Baker, R. C. Crane, and J. B. Howe, J. Opt. Soc. Am. **47**, 240 (1957).
[54] W. W. Piper, D. T. F. Marple, and P. D. Johnson, Phys. Rev. **110**, 323 (1958).
[55] D. T. F. Marple, J. Appl. Phys. **35**, 539 (1964).

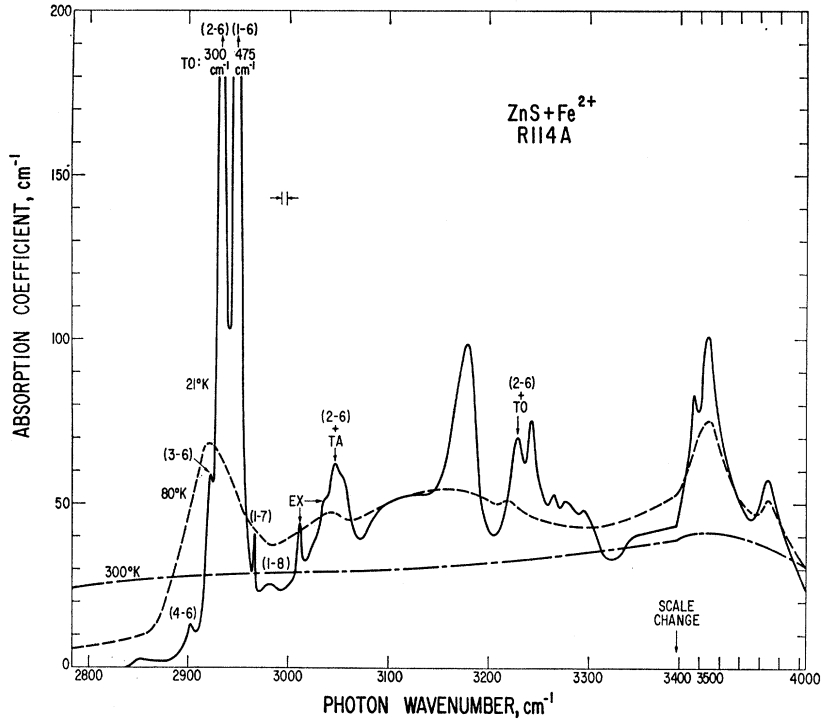

FIG. 2. The optical absorption coefficient, α, versus photon wave number for sample R114A of natural, cubic ZnS containing Fe^{2+}. The spectrum has been taken at 21, 80, and 300°K. The $(A-B)$ designate the zero-phonon optical transitions. In two cases phonon-assisted transitions involving the TA and TO phonons and the (2-6) line can be seen. The two extra peaks labeled EX are probably caused by Fe^{2+} pairs. The spectrometer resolution of 4 cm^{-1} is indicated.

This broad Fe^{2+} absorption band has been studied at low temperatures, where it shows pronounced structure. The results for R114A are shown in Figs. 2 and 3. These measurements were actually carried out for both the R114A and the R118 samples. The α versus $\tilde{\nu}$ curves at 4°K were almost identical, and the complex multipeaked structure in Fig. 3 was the same for both crystals. For this reason, only the results for the R114A

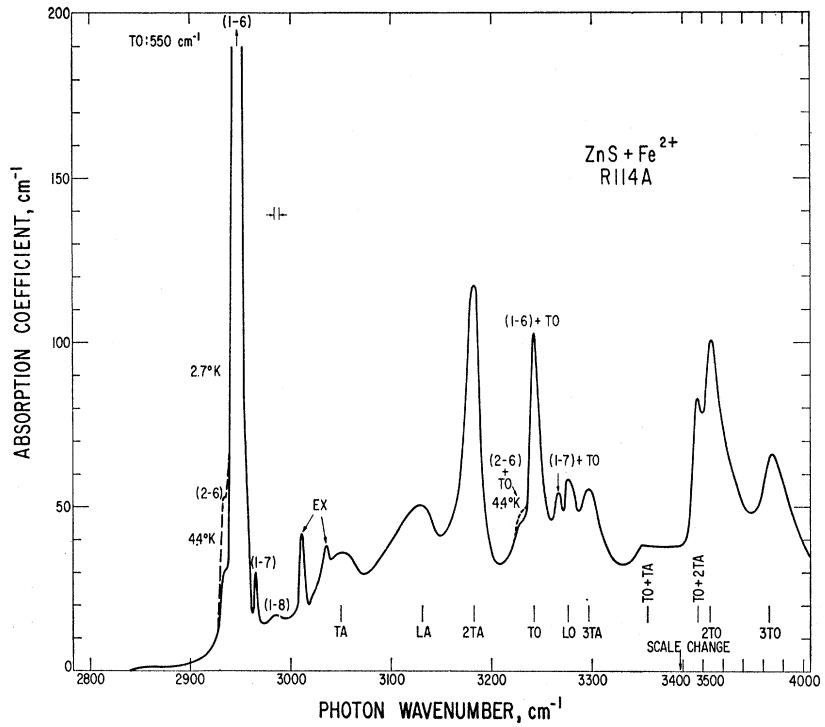

FIG. 3. The optical absorption coefficient α versus photon wave number for sample R114A of natural, cubic ZnS containing Fe^{2+} at 2.7°K and 4.4°K. The $(A-B)$ designate the zero-phonon optical transitions. The dashed lines show the increase in intensity of the (2-6) transition as level No. 2 becomes more populated with increasing temperature. The single and multiple TA, LA, TO, and LO phonon peaks coupled with the (1-6) transition are indicated. The two extra peaks labeled EX are probably caused by Fe^{2+} pairs. The spectrometer resolution of 4 cm^{-1} is indicated.

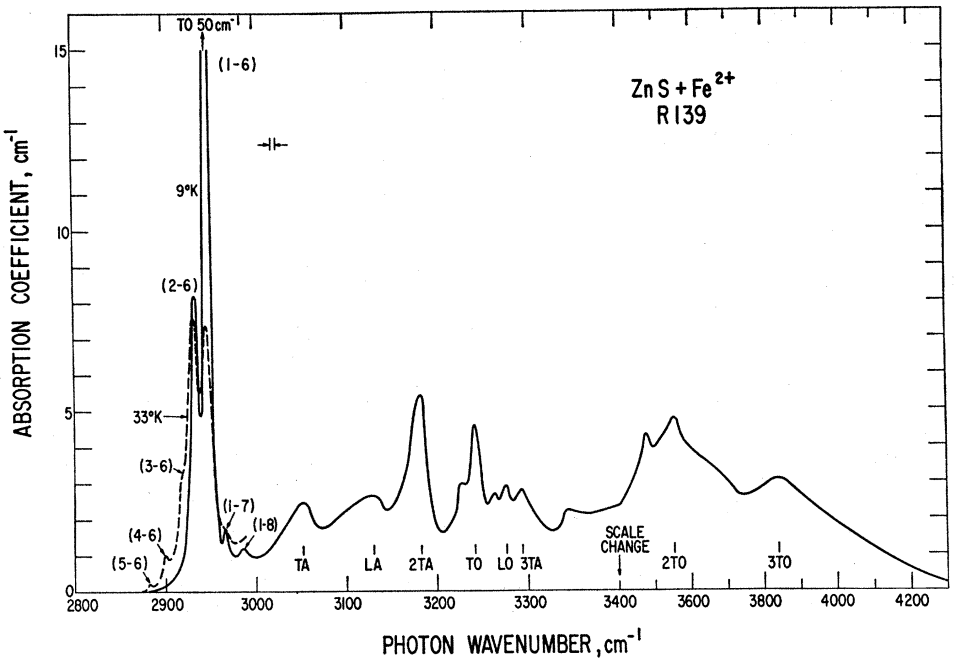

FIG. 4. The optical absorption coefficient α versus photon wave number for sample R139 of natural, cubic ZnS at 9°K and 33°K. The $(A-B)$ designate the zero-phonon lines. Note the similarity to Fig. 3 and the absence of the two EX peaks. The spectrometer resolution of 4 cm^{-1} is indicated.

sample have been shown. The results at 9°K for R139 are shown in Fig. 4. The complex structure is similar to that found for R114A with the exception that the extra peaks (EX in Figs. 2 and 3) at 3012 and 3034 cm^{-1} are absent.

Before describing the structure of this low-temperature Fe^{2+} spectrum in detail, we discuss briefly the rest of the ZnS absorption spectrum in Fig. 1 and show that it is not related to Fe^{2+}. The region between 200 and 1000 cm^{-1} is the reststrahl region, and the optical absorption is produced by interaction of the photons with the lattice phonons. The dashed curve labeled L is the low energy limit of the reststrahl region estimated from the data in the literature.[30,33,56–58] The absorption peaks between 400 and 1000 cm^{-1} are the multiphonon peaks, and the present measurements are in good agreement with those of Deutsch.[30] The next structure in the curves occurs with the band at 14 000 to 16 000 cm^{-1} and is believed to be caused by traces of Co^{2+} in all four samples. The identification as a Co^{2+} absorption is made from a comparison of the results for R140 with those found by Weakliem[11] for Co^{2+} in hexagonal ZnS, where f, the oscillator strength, was 1.3×10^{-2} at 300°K. The calculated value of f for Co^{2+} in R140 for the 15 000 cm^{-1} band is 0.4×10^{-2}, in reasonable agreement with the hexagonal ZnS value. This band has also been seen in natural, cubic ZnS by Low and Weger.[3] The weak band centered at 6800 cm^{-1} in R140 is also caused by Co^{2+}, and matches a similar band in Weakliem's spectrum. Above 20 000 cm^{-1} the measured absorption on these natural, cubic ZnS crystals approaches the intrinsic absorption of ZnS shown as the dashed curve I. This curve has been constructed from data in the literature[59–62] for both high purity cubic and hexagonal ZnS. The difference in α between the measured curve and the curve I suggests that there is another broad absorption band centered near 26 000 cm^{-1}. The cause of this band is uncertain, but it appears to be associated with the presence of iron. Even though iron can exist[63] in ZnS as Fe^{1+}, Fe^{2+}, or Fe^{3+}, it is probable that the Fe^{2+} charge state in these natural crystals is responsible for the absorption. The absorption may be associated with transitions from the ground state to levels derived from the ^3P, ^3H, ^3F, or ^3G free-ion terms of Fe^{2+} which lie between 18 000 cm^{-1} and 25 000 cm^{-1}. The iron absorption in the blue near 26 000 cm^{-1} plus the Co^{2+} absorption in the red cause the yellow color in natural ZnS crystals.

Zero-Phonon Lines of Fe^{2+} in ZnS

The structure in the low-temperature absorption spectrum of Fe^{2+} in ZnS shown in Figs. 2, 3, and 4 arises in part from electronic transitions without phonon

[56] T. Liebisch and H. Rubens, Sitzber. Kgl. Preuss. Akad. Wiss. Berlin, 876 (1919); *ibid.* 211 (1921).

[57] G. Picus. See E. Burstein and P. H. Egli, in *Advances in Electronics and Electron Physics*, edited by L. Marton (Academic Press Inc., New York, 1955), Vol. 7, p. 1.

[58] H. Yoshinaga, Phys. Rev. **100**, 753 (1955).

[59] W. W. Piper, Phys. Rev. **92**, 23 (1953).

[60] S. J. Czysak, D. C. Reynolds, R. C. Allen, and C. C. Reynolds, J. Opt. Soc. Am. **44**, 864 (1954).

[61] W. W. Piper, P. D. Johnson, and D. T. F. Marple, J. Phys. Chem. Solids **8**, 457 (1959).

[62] J. A. Beun and G. J. Goldsmith, Helv. Phys. Acta **33**, 508 (1960).

[63] W. C. Holton, J. Schneider, and T. L. Estle, Phys. Rev. **133**, A1638 (1964).

emission (zero-phonon transitions) between spin-orbit levels of the initial (^5E) and final ($^5T_2$) states of the Fe^{2+}, and in part it arises from phonon-assisted transitions in which one or more phonons are emitted at the same time that the electronic transition takes place. There is, however, no clear way to identify experimentally the type of process to which a given line belongs, apart from the fact that at low temperatures a phonon-assisted transition occurs only at higher energy than the corresponding zero-phonon transition (since the additional energy to emit the phonon must be supplied by the absorbed photon—at sufficiently low temperatures the probability is negligible of phonon-assisted transitions in which a phonon is absorbed). Also, the theory of the energy levels of Fe^{2+} contains uncertainties because of the importance of Jahn-Teller effects (see Sec. IV). Accordingly we must adopt a more or less empirical scheme in labeling the various lines in Figs. 2, 3, and 4. This will now be described. The identification of these transitions in terms of a fundamental model will be the concern of later sections of this paper.

The spectrum of Fig. 4 is the simplest one on which to make this separation. The peaks with $\bar{\nu} \leq 3000$ cm^{-1} are all presumed to be zero-phonon lines for which the initial state is the lowest spin-orbit level of ^5E (the only level appreciably populated at the lowest temperatures) and for which the final state is one of the various levels of $^5T_2$. Peaks with $\bar{\nu} > 3000$ cm^{-1} in Fig. 4, on the other hand, can almost all be fitted by adding the energy of one or more lattice phonons of ZnS to that of one of the zero-phonon lines. Accordingly, most of the peaks with $\bar{\nu} > 3000$ cm^{-1} in Fig. 4 will be presumed to be phonon-assisted lines. The spectra in Figs. 2 and 3 at 2.7°K and higher show two extra lines between 3000 cm^{-1} and 3040 cm^{-1} which are marked EX. These lines are believed to be caused by pairs of Fe^{2+} ions since they occur in the R114A and R118 crystals where the Fe concentration is above 10^{19} cm^{-3}.

The theory of the energy levels of Fe^{2+} (considered in Sec. IV) predicts that the ^5E ground state should consist of five spin-orbit levels which are approximately equally spaced, with a separation of about 10 to 20 cm^{-1} between adjacent levels. The $^5T_2$ upper state, on the other hand, comprises six levels (or possibly more if Jahn-Teller effects complicate the situation). In discussing the level structure inferred from the experimental spectra, therefore, we number the levels of ^5E by $A=1, 2, \cdots, 5$ and those of $^5T_2$ by $B=6, 7, \cdots$ in order of increasing energy. Accordingly, we then designate a zero-phonon line in the experimental spectrum by the label (A-B) according to the (presumed) position in its respective sequence of the initial level (A) and final level (B) between which the transition occurs. Since the fundamental identity of these levels for a given line is left somewhat uncertain by uncertainties in the theory, in describing the experimental spectrum we may regard the designation (A-B) simply as an arbitrary label for a given observed line, the wave number of which is listed in Table II. We must note, in particular, that if an existing level fails for any reason to contribute a distinct zero-phonon line to the spectrum as observed, such a level may be omitted in this empirical numbering scheme.

TABLE II. Zero-phonon lines and their oscillator strengths in the Fe^{2+} $^5E \rightarrow {}^5T_2$ absorption band at low temperatures.

Transition[a]	ZnS[b] Energy,[e] cm^{-1}	ZnS[b] $f\times10^6$[f]	CdTe[c] Energy,[e] cm^{-1}	CdTe[c] $f\times10^6$[f]	$MgAl_2O_4$[d] Energy,[e] cm^{-1}	$MgAl_2O_4$[d] $f\times10^6$[f]
(1-6)	2947	50	2282	6	3595	25
(1-7)	2966	2	2294	7	3660	40
(1-8)	2986	½	2309	8	3731	5
(1-9)		···	2318	5	···	···
(1-10)		···	2334	3	···	···
(2-6)	2932	50	2273	~10	3583	~20
(2-7)	2950±5	<40	···	···	3644	~20
(3-6)	2921	60	2264	20	3570	~20
(4-6)	2901	30	2250	~ 5	3553	~20
(5-6)	2884	10	···	···	···	<10

[a] The optical transitions ($A-B$) are all absorption processes in which the system goes from a lower level A to a higher level B.
[b] The ZnS results are based on a combination of the results of R139 and R114A. The line positions are those found for R114A except for the (5-6) transition where the line at 2282 cm^{-1} in R139 has been shifted to 2284 cm^{-1} to correspond to the 2 cm^{-1} difference in the position of the (1-6) line in the two samples.
[c] The CdTe results are based on sample R121.
[d] The $MgAl_2O_4$ results are based on a combination of those from R54 and R97.
[e] The positions of all absorption lines are given in cm^{-1} and are accurate to about ±2 cm^{-1}.
[f] f = the oscillator strength of a single line calculated from the integrated area under the absorption curve. In the cases where the population of the lower level of the particular transition is temperature-dependent a correction has been made in order to account for the fact that only a fraction of the Fe^{2+} ions are in the level from which the optical transitions takes place. The f values are probably accurate to within a factor of 2. The ~ sign indicates an uncertainty of a factor of about 4.

Since at 2.7°K almost all of the Fe^{2+} ions should be in their lowest level (i.e., No. 1), the zero-phonon lines present at 2.7°K in Fig. 3 are labeled (1-B), with $B=6$, 7, ··· in order of increasing wave number of the line. The strong line that initiates the structure is thus presumed to have the lowest level of $^5T_2$ as its final state, and its designation is therefore (1-6). It lies at 2945±2 cm^{-1} for sample R139, at 2947±2 cm^{-1} for R114A, and at 2952±2 cm^{-1} for R118. In the two crystals R114A and R118 its width at half-maximum is 7 cm^{-1}; in R139 where the Fe^{2+} concentration is less, its width is 4 cm^{-1} at the lowest temperature studied. The other two zero-phonon lines in Fig. 3 at ~0°K are then lines (1-7) and (1-8). These lie so close in energy to line (1-6) that they are not believed to be phonon-assisted transitions derived from (1-6).

As the crystal is warmed up to 4.4°K a line begins to appear at 2932 cm^{-1} (Fig. 3), on the low-energy side of (1-6), and at 21°K (Fig. 2) this line has intensity comparable to (1-6). Presumably this line arises from transitions from level No. 2 to level No. 6, the population of level No. 2 increasing as the temperature rises. This line is therefore labeled (2-6). Similarly, at 21°K (Fig. 2) two other lines (3-6) and (4-6) have begun to appear at energies still lower than (2-6), corresponding

TABLE III. Energy levels of Fe^{2+} in tetrahedral sites in several crystals, as inferred from the experimental optical absorption spectra.[a]

Level number	ZnS Observed	ZnS Calculated[b]	CdTe Observed	CdTe Calculated[b]	$MgAl_2O_4$ Observed	$MgAl_2O_4$ Calculated[b]
1	0	0	0	0	0	0
2	15±2	15	8±3	10	12±2	13
3	27±2	30	18±2	20	25±2	26
4	46±2	45	32±3	30	42±3	39
5	63±2	60	···	40	···	52
6	0	0	0	0	0	0
7	19±2	17.2	12±2	···	64±2	···
8	39±3	41.8	27±2	···	136±3	···
9	···	···	36±2	···	···	···
10	···	···	52±2	···	···	···
E_{16}	2950±3		2282±2		3595±4	

[a] All energies are given in cm^{-1}. The energies of levels No. 2 through No. 5 are given with respect to No. 1 as zero. The energies of levels No. 6 through No. 10 are given with respect to level No. 6 as zero. Level No. 6 lies at an energy E_{16} above level No. 1. The uncertainties in the energies are estimates based on line intensities and breadth as well as on spectrometer resolution.
[b] The values listed for the energies of levels No. 1-5 in the column labeled "calculated" are obtained on the assumption that these levels are uniformly spaced as predicted by crystal-field theory, with an interval 15 cm^{-1} for ZnS, 10 cm^{-1} for CdTe, and 13 cm^{-1} for $MgAl_2O_4$. The "calculated" values or levels No. 7 and No. 8 for ZnS are those given by Table XII of Sec. V.

to the finite population of levels No. 3 and No. 4 at this temperature. At 33°K in R139 the (5-6) line appears (see Fig. 4). With further warming the intensity of these peaks continues to increase, but the spectrum broadens. Almost all of the detailed structure disappears by 80°K (Fig. 2).

The wave numbers and oscillator strengths of these zero-phonon lines are listed in Table II. The oscillator strengths f have been computed from the integrated area under the α-versus-$\bar{\nu}$ curve and the known iron concentration [see Eq. (4.12); the local-field correction is taken[64] as $(\mathcal{E}_{\text{eff}}/\mathcal{E})=(n^2+2)/3$]. The intensities of all the zero-phonon lines in ZnS are proportional to the iron concentration, at least to within the experimental uncertainty of about ±50%.

The relative energies of the levels of ^5E and $^5T_2$, as inferred from the wave number differences of the lines in Table II, are listed in Table III. The spacing of levels No. 1 through No. 5 is nearly constant at 15±2 cm^{-1}.

Phonon-Assisted Lines of Fe^{2+} in ZnS

Most of the lines in the spectrum of Figs. 2, 3, and 4 at energies above 3000 cm^{-1} (except for the lines labelled EX) are presumed to result from absorption processes involving the simultaneous transition of an Fe^{2+} ion from level A to level B and the emission of a phonon. The peaks in the α versus $\bar{\nu}$ curve correspond to peaks in the effective density of states of the phonons interacting with the Fe^{2+} ion. Almost all of the peaks in Figs. 2, 3, and 4 at energies above 3000 cm^{-1} can be

[64] D. L. Dexter, in *Solid State Physics*, edited by F. Seitz and D. Turnbull (Academic Press Inc., New York, 1959), Vol. 6, p. 353.

TABLE IV. Phonon-assisted lines in the Fe^{2+} $^5E \rightarrow {}^5T_2$ absorption band at low temperatures. The energies of the lines are given in cm^{-1}.

Identification of transition[a]	ZnS R114A[b]	ZnS R139	CdTe R121
(2-6)+TA	3047	···	···
(1-6)+TA	3053	3051	2346
(1-7)+TA	···	···	2355
(1-8)+TA	···	···	2371
(1-6)+LA	3131	3129	2388
(1-7)+LA	···	···	2397
(1-6)+2TA	3183	3182	···
(2-6)+TO	3230	3227	···
(1-6)+TO	3243	3241	2422
(1-7)+TO	3267	3263	2434
(1-8)+TO	···	···	2448
(1-6)+LO	3278	3276	2463
(1-7)+LO	···	···	2473
(1-6)+3TA	3297	3293	···
(1-6)+TA+TO	3355	3342	···
(1-6)+2TA+TO	3475	3474	···
(1-6)+2TO	3540	3555	2580
(1-7)+2TO	···	···	
(1-8)+2TO	···	···	
(1-6)+3TO	3850	3840	

[a] The identification of the transition giving rise to each line is based on Eq. (3.1), the observed energies of the zero-phonon lines, and the (derived) set of phonon energies given in Table V (ZnS) or VII (CdTe).
[b] The energies of all the lines including the (1-6) and (1-7) transitions in sample R114A are about 2 cm^{-1} higher than those in R139.

identified, as we shall see, as an absorption involving a zero-phonon transition (A-B) and one or more of the phonons TA, LA, TO, LO of the ZnS host lattice. (TA indicates transverse acoustic, LA indicates longitudinal acoustic, TO indicates transverse optic, LO indicates longitudinal optic.) The peak energy is equal to

$$E_{\text{peak}}=E_{AB}+E_{\text{phn}}, \tag{3.1}$$

where E_{AB} is the no-phonon transition energy and E_{phn} is the energy of the phonon density-of-states maximum. The several peaks and their identifications are given in Table IV. Some of the peaks associated with the (1-6) transition are labeled in Fig. 3. The energies of the four phonons obtained from Table IV are given in Table V.

The four phonon energies in Table V derived from the present experiment are compared with previous data in the literature for the phonons of pure ZnS. The literature data for phonons near the zone boundary are derived from multiphonon bands in the reststrahl region,[30,31] from calculations of the dispersion curves,[28,29] and from optical absorption measurements on Mn^{2+}-doped ZnS.[18,20] The zone-center phonons are taken from Raman-effect studies and from infrared measurements.[30,32,34] The peaks in the phonon density of states probably occur[65] at the Brillouin-zone boundaries, and hence the present results correspond to these values. The zone-center energies are included for comparison purposes. The TO branch has nearly the same energy at

[65] M. Blackman, in *Encyclopedia of Physics*, edited by S. Flügge (Springer Verlag, Berlin, 1955), Vol. 7, Part 1, p. 325.

TABLE V. Phonon energies[a,b] for cubic ZnS in cm^{-1}.

Phonon	Present value	Ref. 20	Ref. 28	Ref. 29	Ref. 30	Ref. 31 No. (2)[c]	Ref. 31 (No. 1)[c]	Refs. 30 and 34	Ref. 32[d]	Ref. 33[d]
TA	115±5	86±5	110±20	110±20	228	115±2	93±2	···	···	···
LA	184±4	···	242±6	205±5	263	190±5	155±5	···	···	···
TO	296±3	298±4	···	320±20	297	298±2	298±2	312	274	273
LO	331±3	340±5	···	320±20	379	339±2	339±2	386	349	355
	Density of states maxima							At zone center		

[a] TA = transverse acoustic, LA = longitudinal acoustic, TO = transverse optic, LO = longitudinal optic.
[b] The limits of error for the present values are those needed to explain the slightly different energies derived from different peaks. The limits on the literature values were not given in the original articles, but have been estimated as those necessary to include the range of values given.
[c] Marshall and Mitra give two different sets of phonon energies, No. 1 and No. 2.
[d] Similar values have been reported also by M. Balkanski, M. Nosimovici, and R. LeToullec, J. Phys. 25, 305 (1964) (TO = 274 cm^{-1}, LO = 350 cm^{-1}), and by A. Mitsuishi, H. Yoshinaga, K. Yata, and A. Manabe, J. Appl. Phys. Japan 4, Suppl. 1, 581 (1965) (TO = 280 cm^{-1} at 300°K).

the center and the edge of the zone; the LO branch has a lower energy at the zone edge.[66] The phonon energies derived in the present experiment are in generally good agreement with previous results in the literature. The disagreement with the TA value of 86 cm^{-1} of Langer and Ibuki[20] derived from optical absorption studies in Mn^{2+} in ZnS is not understood. Their TA value is lower than any of the other values in the literature except for assignment No. 1 of Marshall and Mitra[31] (see Table V).

The area under the α versus $\bar{\nu}$ curves in Fig. 3 has been integrated in order to determine the total oscillator strength F_{tot} of the whole band derived from the ^5D free-ion term of Fe^{2+}. The low-temperature value of F_{tot}, designated by $F_{tot}(\sim 0°K)$ is 6.4×10^{-4} for Fe^{2+} in ZnS, R114A. Nearly the same values were found for R118 and R139. The integrated area under the 2000 to 5000 cm^{-1} peak in Fig. 1 at 300°K gave $F_{tot}(300°K) = 6.7\times10^{-4}$. The fraction (F_0/F_{tot}) of the total absorption associated with the zero-phonon lines having $\bar{\nu}<3000$ cm^{-1} is given in Table VI, as well as the fractions (F_1/F_{tot}), (F_2/F_{tot}), (F_3/F_{tot}) associated with phonon-assisted transitions involving one, two, and three phonons (as identified in Fig. 3 and Table IV). At the lowest temperature of 2.7°K the zero-phonon lines having $\bar{\nu}<3000$ cm^{-1} account for 8% of the total intensity in ZnS. [The values given for F_1, F_2, F_3 in Table VI thus include the contribution to the intensity from any zero-phonon lines that may lie in the energy range $\nu>3000$ cm^{-1} and which either are not resolved

TABLE VI. Total and partial oscillator strengths of the Fe^{2+} $^5E \rightarrow {}^5T_2$ optical absorption band.

$F_{tot}(300°K)$ = total oscillator strength of the $^5E \rightarrow {}^5T_2$ band at 300°K.
$F_{tot}(\sim 0°K)$ = total oscillator strength of the band at low temperatures (2.7°K for ZnS, 3.5°K for CdTe, 6.9°K for $MgAl_2O_4$).
F_0/F_{tot} = partial contribution to $F_{tot}(\sim 0°K)$ from zero-phonon processes.[a]
F_1/F_{tot} = partial contribution to $F_{tot}(\sim 0°K)$ from one-phonon process.[a]
F_2/F_{tot} = partial contribution to $F_{tot}(\sim 0°K)$ from two-phonon processes.[a]
F_{3+}/F_{tot} = partial contribution to $F_{tot}(\sim 0°K)$ from three- and higher-phonon processes.[a]

Oscillator Strength	ZnS	CdTe	$MgAl_2O_4$
$F_{tot}(300°K)\times10^4$	6.7	2.3	5.0
$F_{tot}(\sim 0°K)\times10^4$	6.4	1.8	5.0
F_0/F_{tot}	8%	16%	15%
F_1/F_{tot}	18%	29%	25%
F_2/F_{tot}	33%	32%	60%
F_{3+}/F_{tot}	41%	23%	

[a] The type of process associated with the various peaks is identified in Tables II and IV.

[66] S. S. Mitra, Phys. Rev. 132, 986 (1963).

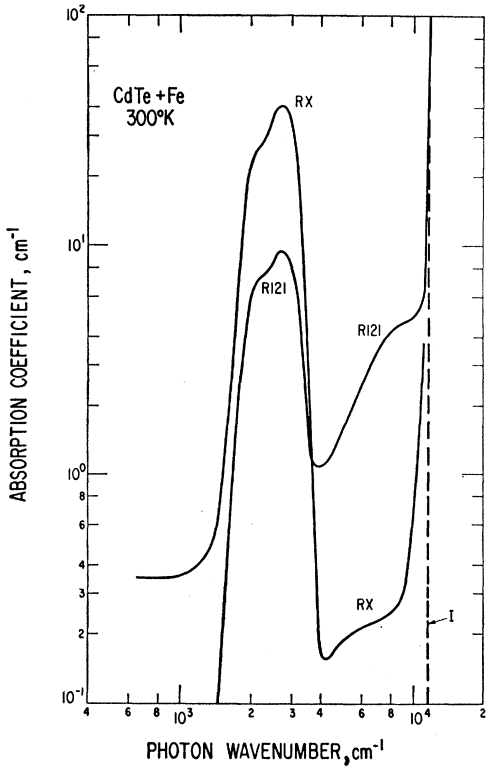

FIG. 5. The optical absorption coefficient α versus photon wave number at 300°K for two crystals of synthetic CdTe doped with iron. The absorption peak in the infrared caused by Fe^{2+} is between 1500 and 4000 cm^{-1}. The dashed curve I shows the absorption edge of pure, undoped CdTe. The spectrometer resolution is 8 cm^{-1}.

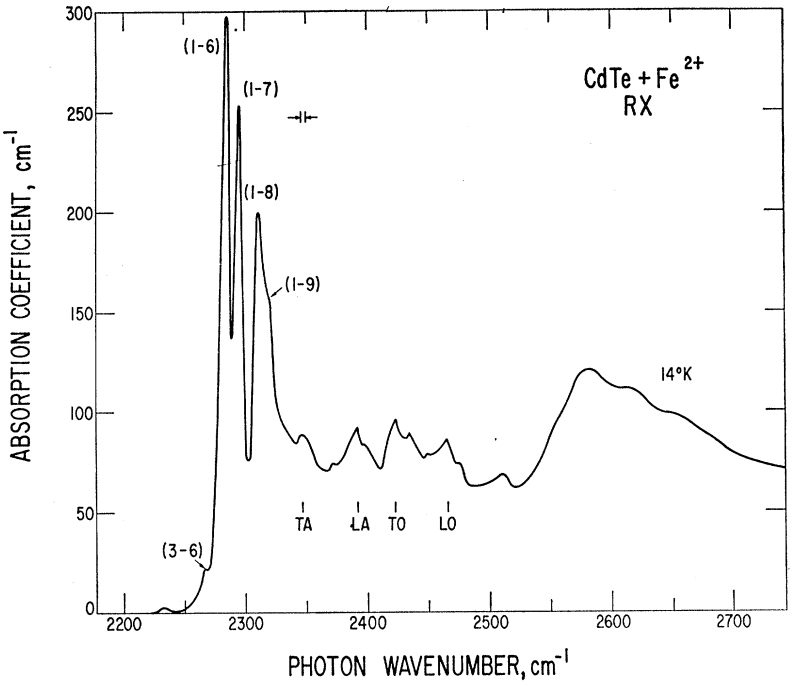

FIG. 6. The optical absorption coefficient α versus photon wave number of the Fe^{2+} peak in CdTe sample RX at 14°K. The $(A-B)$ are the zero-phonon transitions. The TA, LA, TO, and LO are the phonon peaks associated with the (1-6) transition. The spectrometer resolution of 4 cm^{-1} is indicated. The α values >200 cm^{-1} are approximate.

as peaks or have been incorrectly identified as phonon-assisted lines.]

B. Cadmium Telluride

The optical absorption spectrum of Fe^{2+} in CdTe is somewhat similar to that of Fe^{2+} in ZnS. This might have been expected, since the Fe^{2+} substitutes[25] for Cd^{2+}, and since cubic ZnS and CdTe have the same crystal structure. Figure 5 shows the results at 300°K for the optical absorption coefficient of the two synthetic single crystals of Fe^{2+}-doped CdTe from 600 to 12 000 cm^{-1}. The intrinsic absorption of undoped CdTe as measured by Marple and Segall[67] is shown as the dashed

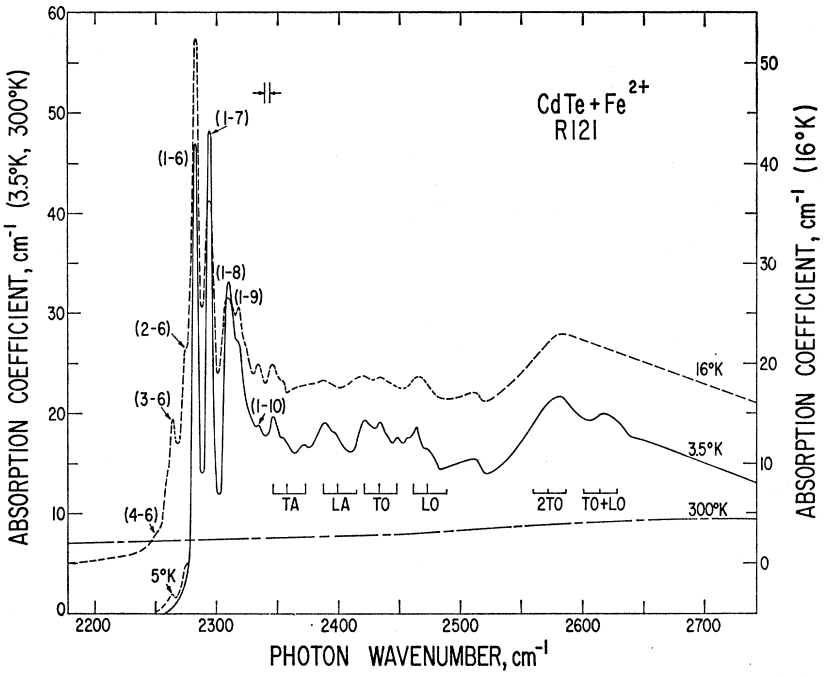

FIG. 7. The optical absorption coefficient α versus photon wave number of the Fe^{2+} peak in CdTe sample R121 at several temperatures. Note the vertical offset of the 16°K curve. The $(A-B)$ designate the zero-phonon optical transitions. The phonon-assisted transitions involving TA, LA, TO, and LO phonons are shown. Each of the single phonon peaks is a triplet involving the three zero-phonon lines (1-6), (1-7), and (1-8). However, for LA and LO the (1-8) peak does not show up. The spectrometer resolution of 4 cm^{-1} is indicated.

[67] D. T. F. Marple and B. Segall, Bull. Am. Phys. Soc. 9, 223 (1964).

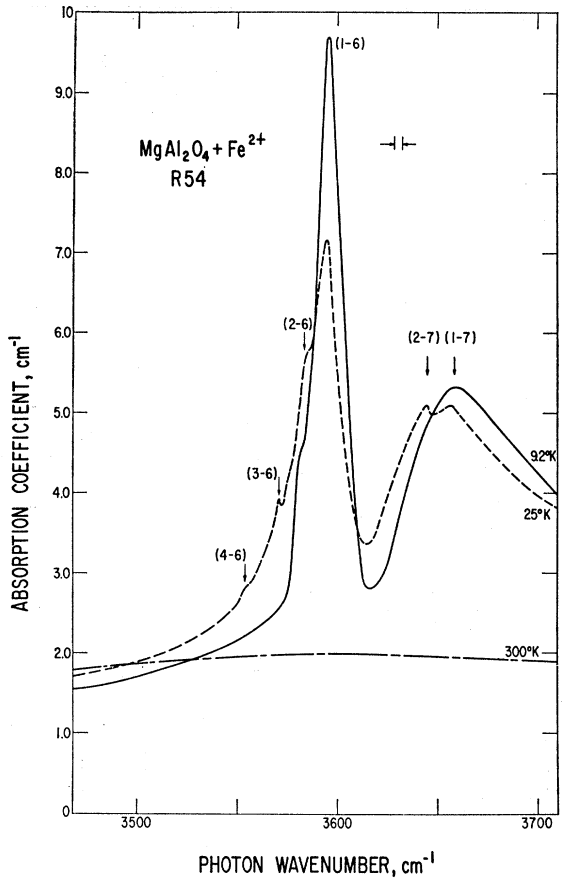

FIG. 8. The optical absorption coefficient α versus photon wave number of the Fe^{2+} peak in a natural $MgAl_2O_4$ crystal R54 at several temperatures. The $(A-B)$ designate the zero-phonon optical transitions. The spectrometer resolution of 4 cm^{-1} is indicated.

line I at 12 000 cm^{-1} (see also Davis and Shilliday).[68] The reststrahl band in CdTe lies below 400 cm^{-1}, and does not show up in Fig. 5 as it does for ZnS in Fig. 1. The only absorption that can be attributed to the Fe^{2+} ion is the broad band between 1500 and 4000 cm^{-1}. The background absorption, particularly in sample R121, is presumed to be caused by some other impurity. By comparing the results for the two samples, it can be seen that the absorption coefficient in the 1500 to 4000 cm^{-1} band is proportional to the iron concentration.

The Fe^{2+} absorption in both RX and R121 has been studied at low temperatures. The results are quite similar, and are shown in Figs. 6 and 7. Adopting a labeling scheme like that used for the zero-phonon lines of Fe^{2+} in ZnS, we obtain for these transitions the wave numbers listed for CdTe in Table II. The zero-phonon transitions (1-6) and (1-7) were both well resolved at 3.5°K for sample R121 in Fig. 7. In sample RX the Fe^{2+} concentration was so large that the sample became optically opaque at these transitions; therefore the high absorption ends (above $\alpha = 200$ cm^{-1}) of (1-6) and (1-7) in Fig. 6 have been estimated.

[68] P. W. Davis and T. S. Shilliday, Phys. Rev. **118**, 1020 (1960).

TABLE VII. Phonon energies for CdTe in cm^{-1}.

Phonon[a]	Present value	Ref. 35	Ref. 36	Ref. 37
TA	65±3			
LA	105±3			
TO	140±3		140	144
LO	180±3	172	170[b]	
	Density-of-states maxima		At zone center	

[a] TA indicates transverse acoustic, LA indicates longitudinal acoustic, TO indicates transverse optic, LO indicates longitudinal optic.
[b] Calculated by Halsted *et al.* (Ref. 35) from TO of Fisher and Fan [Ref. 36].

The spectrum for CdTe is somewhat more complex than that for ZnS because there are several zero-phonon lines of comparable strength. The (1-6) transition occurs at 2282±2 cm^{-1} for R121 and 2284±3 cm^{-1} for RX, and for R121 at 3.5°K has a width of 5 cm^{-1} at an α value of half maximum. Table II gives the oscillator strengths of the various zero-phonon transitions. Even though samples RX and R121 differ in iron concentration by a factor of 5, the oscillator strengths for a given line do not differ by more than a factor of 1.5 for the two samples. Thus the absorption coefficient for these lines is proportional to the iron concentration to within the experimental error. The oscillator strengths in Table II for CdTe are of the same order of magnitude as those for ZnS. The major difference is that in ZnS the (1-6) transition is much stronger than the (1-7) and (1-8) transitions, whereas in CdTe the three are of comparable strength. There are also two weaker zero-phonon lines, (1-9) and (1-10), which appear in CdTe but not in ZnS. The relative positions of the energy levels of Fe^{2+} in CdTe, as derived from Table II, are given in Table III. Levels No. 1–No. 4 are spaced approximately uniformly, as expected from theory, with a separation 10±2 cm^{-1}. Levels No. 6–No. 10 also appear to be spaced nearly uniformly, with a separation of 12±2 cm^{-1}.

The phonon-assisted lines of the spectrum (Table IV) are analyzed using the same procedure as that found to be successful for ZnS. The demarcation point between zero-phonon and phonon-assisted transitions is believed to be near $\bar{\nu} = 2340$ cm^{-1}. This division yields quite reasonable values for the phonon energies (Table VII) which we have labeled TA, LA, TO, and LO, and we find (Figs. 6 and 7) a repetitive pattern of three lines, for each of these four phonons, which resembles the pattern of the three zero-phonon lines (1-6), (1-7), and (1-8). The present values for the TA, LA, TO, and LO energies are listed in Table VII together with previous values available from the literature for the phonons of pure CdTe.[34–36] The agreement for the optical phonons is reasonable. No previous data on the acoustic phonons in CdTe is known.

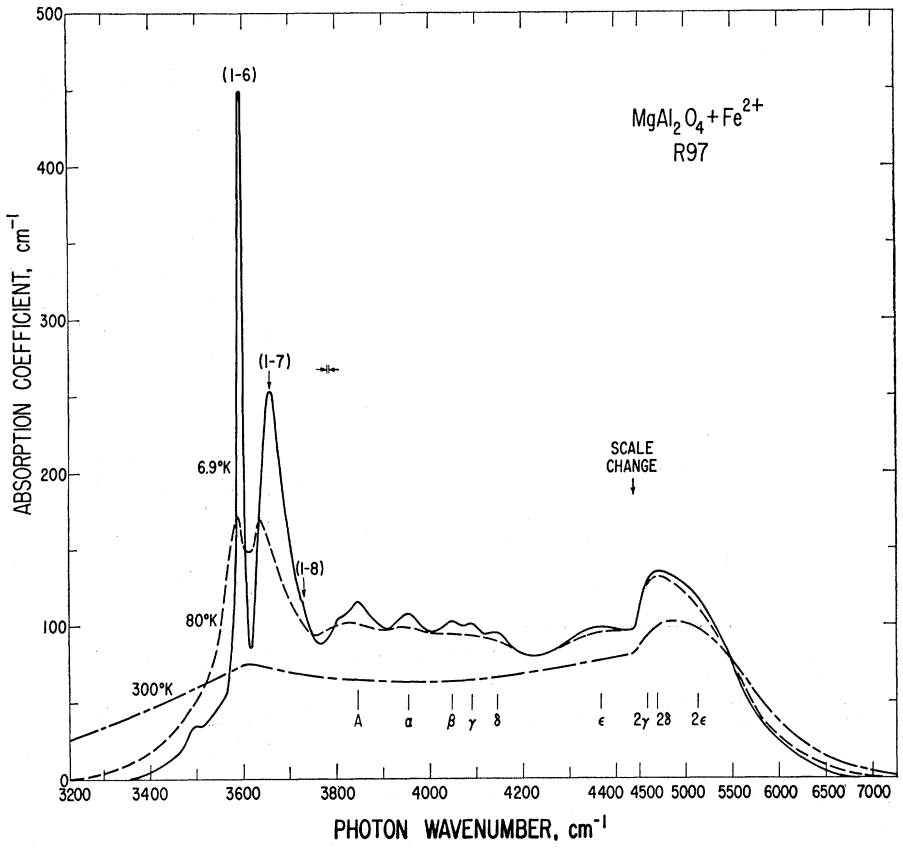

FIG. 9. The optical absorption coefficient α versus photon wave number of the Fe^{2+} peak in a natural $MgAl_2O_4$ crystal R97 at 6.9°K. The results for 80°K and 300°K are also shown. The $(A-B)$ designate the zero-phonon optical transitions. The single and multiple phonon peaks involving A, α, β, γ, δ, and ϵ phonons that are coupled with the (1-6) transition are indicated. The spectrometer resolution of 4 cm^{-1} is indicated.

From the identification of the phonon peaks in Fig. 7, it is now possible to integrate the absorption curve in order to determine the fractional contribution from the various one- and two-phonon processes as well as the total oscillator strength for the whole band. Table VI gives these numbers. The zero-phonon part contributes 16% of the total intensity at 3.5°K, amd the most probable number of phonons emitted is 2. The total oscillator strength for Fe^{2+} in CdTe is about $\frac{1}{3}$ of that for Fe^{2+} in ZnS.

C. Magnesium Aluminate

The infrared optical absorption band caused by Fe^{2+} ions in $MgAl_2O_4$ at 300°K has been reported in a previous paper[19] for both R54 and R97. The Fe^{2+} ion substitutes for the Mg and occurs in the tetrahedral sites. Little, if any, Fe^{2+} occurs in the octahedral Al sites.[19] The low-temperature results are shown in Figs. 8 and 9. The zero-phonon peaks are labeled as before, and the (1-6) transition occurs at 3595 ± 4 cm^{-1} for both crystals. Its half-width is 15 cm^{-1}. This is about three times as large as the half-width values for ZnS and CdTe and makes observation of the (2-6), (3-6), and (4-6) transitions more difficult. The (5-6) transition was not observed at its calculated energy of 3540 cm^{-1}. The other zero-phonon transitions are listed in Table II together with their oscillator strengths. The demarcation between zero-phonon and one-phonon lines has been taken as 3770 cm^{-1}. The (1-7) transition is stronger than (1-6), in contrast to the ZnS. The positions of the A and B levels are given in Table III. The levels No. 1 through No. 4 have an equal spacing of 13 ± 2 cm^{-1}.

The phonon-assisted transitions in $MgAl_2O_4$ are clearly present for R97 in Fig. 9. They were also present for R54, but were not plotted because the results for R54 and R97 were essentially similar, the absorption coefficient being proportional to the iron concentration.

TABLE VIII. Phonon energies for $MgAl_2O_4$ in cm^{-1}.

Peak[a]	Present value cm^{-1}	Literature[b] cm^{-1}
A	220	...
α	365	302
β	450	475
γ	500	530
δ	550	580
ϵ	775	735

[a] The letter A denotes what is probably an acoustic phonon energy. The Greek letters denote what are probably optical phonons. (See discussion in text.)

[b] These values correspond to peaks in the normal incidence reflectivity of a natural crystal of $MgAl_2O_4$. (See Ref. 19.)

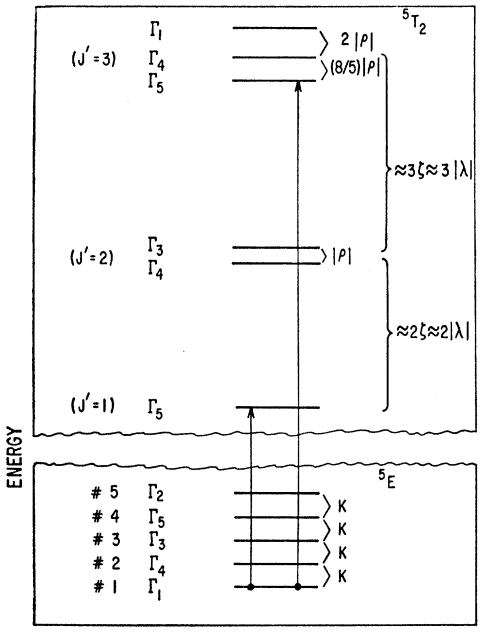

FIG. 10. The energy levels (schematic) of Fe^{2+} ($3d^6$) as predicted by static crystal-field theory for tetrahedral coordination (T_d). The arrows indicate the two optical transitions from the lowest level (Γ_1) of ^5E which are electric-dipole allowed.

The identification of the phonons in the complex spinel lattice is not easy, and no definite assignments have been made. The peak labeled A appears to be associated with acoustic phonons that assist a (1-6) or a (1-7) transition. The phonon energy so derived is about 220 cm^{-1}, and is comparable to the zone-boundary energies for acoustic phonons in the related crystal, MgO.[38] The other phonon-assisted peaks shown in Fig. 9 correspond approximately to the peaks seen in the optical reflectivity.[19] A comparison of the two is made in Table VIII, where the present values have been derived by assuming that the phonon-assisted transitions are related to the (1-6) zero-phonon transition.

The oscillator strength of the Fe^{2+} band is given in Table VI, and is comparable to that in ZnS and CdTe. The most probable number of emitted phonons is 2, and the zero-phonon part of the spectrum contributes 15% of the integrated intensity of the band at 6.9°K.

IV. ENERGY-LEVEL SCHEME FOR TETRAHEDRAL Fe^{2+}-THEORY

The purpose of this section is to set forth what can be expected on theoretical grounds for the energy-level scheme and optical transition intensities of tetrahedral Fe^{2+}. The conventional crystal-field (or ligand-field) model is considered first, and electronic energy levels and oscillator strengths are obtained for an Fe^{2+} ion in a static crystalline environment. We then consider the dynamical coupling between electronic motions and lattice vibrations (e.g., Jahn-Teller effects) and the resulting changes in the energy level scheme of the coupled vibronic (vibrational-electronic) system. Since a complete theory of the dynamical Jahn-Teller effects in a crystalline lattice has not yet been worked out, and since the electron-lattice coupling parameters are not known for tetrahedral Fe^{2+}, these considerations do not lead to a definitive prediction of a detailed model. However, under suitable restrictions the theory does predict the general form of a phenomenological model for the vibronic energy levels and transition intensities. This model is obtained in this section and then used in Sec. V to fit many of the experimental results.

A. Static Crystal-Field Model

At a site of tetrahedral symmetry (T_d), the lowest free ion term, ^5D, of Fe^{2+} ($3d^6$) is split by the crystalline field into an orbital doublet ^5E and triplet $^5T_2$.[69] Crystal-field theory[22,70] predicts that ^5E is the ground state and that $^5T_2$ is higher in energy by $\Delta \approx 10|Dq|$, where Dq is the one-electron cubic-field parameter. Optical studies[1–21] of tetrahedrally coordinated divalent iron-group ions in oxides and sulfides have determined $|Dq|$ to be ≈ 300 to ≈ 600 cm^{-1}; somewhat similar values of $|Dq|$ for tellurides and selenides may be estimated[71] from data on g shifts. Since the higher states of Fe^{2+} are expected[72,73] to be $\gtrsim 18\,000$ cm^{-1} above ^5E when $|Dq|$ is so relatively small, the only optical transition below $\approx 18\,000$ cm^{-1} expected from tetrahedral Fe^{2+} is therefore the $^5E \rightarrow {}^5T_2$ transition in the range ≈ 2000 to ≈ 6000 cm^{-1}. This transition has previously been identified by Pappalardo and Dietz[7] for Fe^{2+} in CdS as centered at 2800 cm^{-1} and by Low and Weger[3] for Fe^{2+} in cubic ZnS at 3300 cm^{-1}.

Fine structure in the $^5E \rightarrow {}^5T_2$ transition should appear because of the splitting of the ^5E and $^5T_2$ terms due to first- and second-order spin-orbit coupling. This splitting has been calculated by Low and Weger[3]; we shall describe it here in terms of a phenomenological model which permits some generalization beyond Low and Weger's considerations.

[69] We denote the irreducible representations of T_d using the notation (A_1,A_2,E,T_1,T_2) of Mulliken [R. S. Mulliken, Phys. Rev. 43, 279 (1933)] for orbital states, crystal-field terms, vibrational states, modes of vibration, and orbital vibronic states (product states made up of electronic orbital wave functions and vibrational wave functions). We use the corresponding notation (Γ_1,Γ_2,Γ_3,Γ_4,Γ_5) of Bethe [H. E. Bethe, Ann. Physik 3, 133 (1929)] for spin-orbit states arising from either electronic or vibronic orbital states through inclusion of spin, account being taken of spin-orbit splitting. The character table defining these representations may be found in Griffith's book (Ref. 22, Table A5, p. 383).

[70] D. S. McClure, in *Solid State Physics* edited by F. Seitz and D. Turnbull (Academic Press Inc., New York, 1959), Vol. 9, p. 399.

[71] F. S. Ham and G. W. Ludwig, in *Proceedings of the First International Conference on Paramagnetic Resonance, Jerusalem, 1962* (Academic Press Inc., New York, 1963), Vol. I, p. 130.

[72] *Atomic Energy Levels*, edited by C. E. Moore, Nat. Bur. Std. (U.S) Circ. No. 467 (U. S. Government Printing and Publishing Office, Washington, D. C., 1952), Vol. 2, p. 60.

[73] Y. Tanabe and S. Sugano, J. Phys. Soc. (Japan) 9, 766 (1954).

The ^5E ground term is not split to first order in the spin-orbit interaction. In second order it splits into five equally spaced levels with the relative energies

$$\begin{aligned} &\text{No. 1 } \Gamma_1 \quad E=-4K \\ &\text{No. 2 } \Gamma_4 \quad E=-3K \\ &\text{No. 3 } \Gamma_3 \quad E=-2K \\ &\text{No. 4 } \Gamma_5 \quad E=-K \\ &\text{No. 5 } \Gamma_2 \quad E=0 \end{aligned} \tag{4.1}$$

as shown in the lower part of Fig. 10. K has been given by Low and Weger[3] to be

$$K=6\lambda^2/\Delta, \tag{4.2}$$

and Γ_1 is the ground state if K is positive, as it should be for tetrahedral Fe^{2+}. In Eq. (4.2), λ is the parameter specifying the Fe^{2+} spin-orbit interaction $\lambda(\mathbf{L}\cdot\mathbf{S})$ within the states derived from ^5D, and the coupling considered in deriving Eq. (4.2) is that between ^5E and $^5T_2$. For free-ion wave functions,[72] $\lambda\approx-(100\pm10)$ cm^{-1} for Fe^{2+}. More generally, one can show from group theory that in cubic or tetrahedral symmetry the level spacing of ^5E remains uniform as long as one admits no terms of third or higher order in the spin operators S_x, S_y, S_z in setting up the effective Hamiltonian of the ^5E states. The value of K may be modified from that given in Eq. (4.2) not only through changes in the effective spin-orbit coupling between ^5E and $^5T_2$ due to overlap and covalent effects [these simply change the value of λ entering Eq. (4.2)], but also through spin-spin interaction and through spin-orbit coupling to states other than $^5T_2$—in particular the $S=1$ states of Fe^{2+} at $\gtrsim18\,000$ cm^{-1}. In addition, a reduction in the magnitude of K may be caused by a dynamical Jahn-Teller effect. This possibility will be treated later.

The spin-orbit splitting of $^5T_2$ in cubic or tetrahedral symmetry may be described conveniently by the phenomenological Hamiltonian

$$\begin{aligned} \mathcal{H}_{so}(^5T_2)=&\zeta(\mathfrak{L}\cdot\mathbf{S})+\mu(\mathfrak{L}\cdot\mathbf{S})^2 \\ &+\rho(\mathfrak{L}_x^2S_x^2+\mathfrak{L}_y^2S_y^2+\mathfrak{L}_z^2S_z^2), \end{aligned} \tag{4.3}$$

which includes all possible terms of first and second order in S_x, S_y, S_z but omits the small terms of third and fourth order. Here $\mathfrak{L}=(\mathfrak{L}_x,\mathfrak{L}_y,\mathfrak{L}_z)$ (x, y, z denote the *cubic* axes) is an Hermitian effective orbital angular momentum operator[74] defined such that its only nonzero matrix elements are the following ones between the three real orbital states[75] $|T_2\xi\rangle$, $|T_2\eta\rangle$, $|T_2\zeta\rangle$ of $^5T_2$:

$$\begin{aligned} \langle T_2\eta|\mathfrak{L}_x|T_2\zeta\rangle&=\langle T_2\zeta|\mathfrak{L}_y|T_2\xi\rangle \\ &=\langle T_2\xi|\mathfrak{L}_z|T_2\eta\rangle=-i. \end{aligned} \tag{4.4}$$

Defining the effective total angular momentum operator $\mathbf{J}$ by

$$\mathbf{J}=\mathfrak{L}+\mathbf{S}, \tag{4.5}$$

which for $^5T_2$ has the eigenvalues $J'=1$, 2, 3, we may express $(\mathfrak{L}\cdot\mathbf{S})$ as

$$\mathfrak{L}\cdot\mathbf{S}=\tfrac{1}{2}(\mathbf{J}^2-\mathbf{S}^2-\mathfrak{L}^2). \tag{4.6}$$

Accordingly, all of $\mathcal{H}_{so}(^5T_2)$ in Eq. (4.3) except the last term is a function only of J^2; the last term splits the $J'=2$, 3 levels and also couples the two pairs of Γ_4 and Γ_5 levels. Assuming ρ to be small and ignoring this latter coupling, we obtain for the relative energies of the levels of $^5T_2$

$$\begin{aligned} J'=1\ \ &\Gamma_5 \quad E=-3\zeta+9\mu+(27/5)\rho \\ J'=2\ \ &\Gamma_3 \quad E=-\zeta+\mu+2\rho \\ &\Gamma_4 \quad E=-\zeta+\mu+3\rho \\ J'=3\ \ &\Gamma_1 \quad E=+2\zeta+4\mu+2\rho \\ &\Gamma_4 \quad E=+2\zeta+4\mu+4\rho \\ &\Gamma_5 \quad E=+2\zeta+4\mu+(28/5)\rho. \end{aligned} \tag{4.7}$$

These levels are represented in the upper part of Fig. 10, where the assumption is made that ζ is positive, ρ negative, and $\zeta\gg|\mu|$, $|\rho|$.

Values for the parameters ζ, μ, and ρ may be obtained from the work of Low and Weger[3] if we consider only spin-orbit coupling between $^5T_2$ and ^5E. We obtain

$$\begin{aligned} \zeta&=-\lambda+2\lambda^2/\Delta, \\ \mu&=+2\lambda^2/\Delta, \\ \rho&=-6\lambda^2/\Delta. \end{aligned} \tag{4.8}$$

Other contributions to ζ, μ, and ρ arise from spin-orbit coupling to $S=1$ states of the configurations $t_2^ne^{6-n}$ with $n=3$, 4, 5, but since for tetrahedral Fe^{2+} such states lie $\gtrsim15\,000$ cm^{-1} above $^5T_2$ these contributions are considerably smaller than those from ^5E. More important corrections to the values of ζ, μ, and ρ in Eq. (4.8) are caused by Jahn-Teller effects (see below).

The over-all optical transition $^5E\rightarrow{}^5T_2$ is both electric- and magnetic-dipole–allowed in tetrahedral symmetry. The odd part of the tetrahedral crystal field breaks down the parity selection rule which would

TABLE IX. Selection rules for optical transitions in tetrahedral (T_d) symmetry.[a]

Initial state		Final state				
Electric-dipole transition	Magnetic-dipole transition	Γ_1	Γ_2	Γ_3	Γ_4	Γ_5
Γ_1	Γ_2	F	F	F	F	A
Γ_2	Γ_1	F	F	F	A	F
Γ_3	Γ_3	F	F	F	A	A
Γ_4	Γ_5	F	A	A	A	A
Γ_5	Γ_4	A	F	A	A	A

[a] F = forbidden; A = allowed.

[74] A. Abragam and M. H. L. Pryce, Proc. Roy. Soc. (London) **A205**, 135 (1951).

[75] We use the same notation as that used by Griffith (Ref. 22, p. 226) to label the orbital states according to their transformation properties.

otherwise make the transition electric-dipole–forbidden. However, individual fine-structure components between the spin-orbit levels of ^5E and $^5T_2$ may still be either electric- or magnetic-dipole–forbidden (or both) because of symmetry considerations (see Table IX). For those components which are electric-dipole allowed (and not made weak by a spin selection rule), we expect the electric-dipole part of the transition probability to predominate and the transition to be relatively strong. Other transitions may show up very weakly if they are magnetic-dipole–allowed.

The absorption coefficient $\alpha(\nu)$ due to the Fe^{2+}, for linearly polarized light of frequency ν, takes the form[64,76]

$$\alpha(\nu)=\frac{2\pi^2Ne^2h}{mcn}\left(\frac{\mathcal{E}_{\rm eff}}{\mathcal{E}}\right)^2 \times \mathrm{Av}_A \sum_B f(A,B)\delta(E_B-E_A-h\nu). \quad (4.9)$$

Here N is the number of isolated Fe^{2+} per unit volume, e and m the electron charge and mass, c the speed of light in vacuum, n the real part of the index of refraction of the crystal at frequency ν, and $(\mathcal{E}_{\rm eff}/\mathcal{E})$ the ratio of the effective electric field at the Fe^{2+} site to the average macroscopic field in the crystal. The oscillator strength of the transition from an initial level A (at energy E_A) to the final level B (energy E_B) is denoted by $f(A,B)$. The sum in Eq. (4.9) extends over the final levels B [when the final level B is degenerate we absorb the sum over the degenerate states comprising B into the definition of the oscillator strength $f(A,B)$], and Av_A indicates that the expression is to be averaged over the initial levels according to the prescription

$$\mathrm{Av}_A W(A)=Z^{-1}\sum_A d_A W(A)\exp(-E_A/kT), \quad (4.10)$$

where $Z=\sum_A d_A\exp(-E_A/kT)$, and d_A denotes the degeneracy of level A. The general expression for $f(A,B)$ is

$$f(A,B)=(2/md_Ah\nu_{BA}) \times\sum_{a,b}|\langle Aa|\sum_j(\mathbf{p}_j\cdot\hat{e})e^{i\mathbf{k}\cdot\mathbf{r}_j}|Bb\rangle|^2, \quad (4.11)$$

where $h\nu_{BA}=(E_B-E_A)$, $\mathbf{r}_j$ and $\mathbf{p}_j$ are the position and momentum of the jth electron, $\mathbf{k}$ and $\hat{e}$ are, respectively, the propagation vector of the light wave and a unit vector in the direction of its polarization, and the sums are over all the electrons and over the degenerate states a and b comprising levels A and B, respectively. In terms of the absorption coefficient measured experimentally, if the line arising from the transition $A\rightarrow B$ is well resolved its oscillator strength is given by

$$f(A,B)=\frac{mcn}{\pi e^2N}\left(\frac{\mathcal{E}}{\mathcal{E}_{\rm eff}}\right)^2\frac{Z\exp(E_A/kT)}{d_A}\int\alpha(\nu)d\nu, \quad (4.12)$$

where the integral is over the line.

[76] M. Lax, J. Chem. Phys. **20**, 1752 (1952).

For an electric-dipole transition, Eq. (4.11) simplifies to

$$f_e(A,B)=(4\pi mv_{BA}/\hbar d_A)\sum_{a,b}|\langle Aa|\mathbf{R}\cdot\hat{e}|Bb\rangle|^2, \quad (4.13)$$

where $\mathbf{R}=\sum_j\mathbf{r}_j$. For a purely magnetic-dipole transition we obtain instead

$$f_m(A,B)=(h\nu_{BA}n^2/2mc^2d_A)(\mathcal{E}/\mathcal{E}_{\rm eff})^2 \times\sum_{a,b}|\langle Aa|\mathbf{L}\cdot(\hat{e}\times\hat{k})|Bb\rangle|^2, \quad (4.14)$$

where $\hbar\mathbf{L}$ is the orbital angular-momentum operator, and $\hat{k}$ is a unit vector along $\mathbf{k}$. In writing Eq. (4.14) we have included a factor $(\mathcal{E}/\mathcal{E}_{\rm eff})^2$ to compensate the factor $(\mathcal{E}_{\rm eff}/\mathcal{E})^2$ appearing in Eq. (4.9), since for a magnetic-dipole transition the coupling is with the magnetic vector of the incident light and no local field correction should be made.

For the fine structure components of the transition $^5E\rightarrow{}^5T_2$ in tetrahedral symmetry, as given by crystal-field theory, the matrix elements of $\mathbf{R}$ appearing in Eq. (4.13) may all be expressed as multiples of a single matrix element, the multiplying factors being determined uniquely [we assume, of course, that $|\zeta|\gg|\rho|$ as in Eq. (4.7)]. Accordingly, the relative intensities of the fine-structure components of electric-dipole origin are completely determined by crystal-field theory. The same is true for the matrix elements of $\mathbf{L}$ in Eq. (4.14), so that the relative intensities of components of purely magnetic-dipole origin are similarly fixed. We define therefore the parameters

$$a^2=(2\pi mv_0/\hbar)|\langle E\theta|R_z|T_2\zeta\rangle|^2 \quad (4.15)$$

and

$$b^2=(h\nu_0n^2/4mc^2)(\mathcal{E}/\mathcal{E}_{\rm eff})^2|\langle E\epsilon|L_z|T_2\zeta\rangle|^2 \quad (4.16)$$

in terms of particular matrix elements[75] of $\mathbf{R}$ and $\mathbf{L}$ between the orbital wave functions comprising the ^5E and $^5T_2$ states. Taking ν_0 in Eqs. (4.15) and (4.16) to be an average frequency for the various components, and ignoring the small difference between ν_{BA} and ν_0, we may then express the oscillator strengths (4.13)

TABLE X. Relative oscillator strengths $f_e(A,B)/a^2$ and $f_m(A,B)/b^2$ for electric- and magnetic-dipole transitions between spin-orbit levels of ^5E and $^5T_2$ as given by crystal-field theory.[a]

Initial level A of ^5E		Final level B of $^5T_2$					
Electric-dipole transition	Magnetic-dipole transition	$J'=1$	$J'=2$		$J'=3$		
		Γ_5	Γ_4	Γ_3	Γ_5	Γ_4	Γ_1
Γ_1	Γ_2	$\frac{2}{5}$	0	0	$\frac{3}{5}$	0	0
Γ_4	Γ_5	$\frac{3}{10}$	$\frac{1}{6}$	0	$\frac{1}{5}$	$\frac{1}{3}$	0
Γ_3	Γ_3	$\frac{1}{5}$	$\frac{1}{3}$	0	$\frac{3}{10}$	$\frac{1}{6}$	0
Γ_5	Γ_4	$\frac{1}{10}$	1/18	4/9	1/15	$\frac{1}{9}$	2/9
Γ_2	Γ_1	0	$\frac{2}{3}$	0	0	$\frac{1}{3}$	0

[a] The values given in the table for $f_e(A,B)/a^2$ and $f_m(A,B)/b^2$ have been summed over the degenerate states of the final spin-orbit level B and averaged over those of the initial level A, in accordance with Eqs. (4.13) and (4.14) of the text. The quantities a^2 and b^2 are defined in Eqs. (4.15) and (4.16). The states of $^5T_2$ used in this table are eigenstates of J^2 [Eq. (4.5)] and therefore are eigenstates of $\mathcal{H}_{so}(^5T_2)$ in (4.3) provided that $|\zeta|\gg|\rho|$.

and (4.14) as

$$f_e(A,B)=p_e(A,B)a^2, \tag{4.17a}$$

$$f_m(A,B)=p_m(A,B)b^2. \tag{4.17b}$$

The numbers $p_e(A,B)$ and $p_m(A,B)$ are given in Table X. As we see from this Table, the sum of the oscillator strengths over the final states is the same for each initial level and is given simply by a^2 for an electric-dipole transition and b^2 for a magnetic dipole process. It follows then from Eq. (4.9), when we integrate $\alpha(\nu)$ over all the fine structure lines comprising the ${}^5E\rightarrow{}^5T_2$ absorption band and take account of both types of processes, that

$$\int\alpha(\nu)d\nu=\frac{\pi Ne^2}{mcn}\left(\frac{\mathcal{E}_{\text{eff}}}{\mathcal{E}}\right)^2(a^2+b^2). \tag{4.18}$$

Thus the total oscillator strength F_{tot} of the band is given by the static crystal-field model to be simply

$$F_{\text{tot}}=(a^2+b^2) \tag{4.19}$$

and this result is independent of the temperature.

To estimate the magnitude of these oscillator strengths, we can use for the magnetic-dipole part the value $|\langle E\epsilon|L_z|T_2\zeta\rangle|=2$, which is exact for the ${}^5D$ wave functions of the free ion. Then if $\bar{\nu}_0=(\nu_0/c)=3400$ cm^{-1}, and $n^2=5.1$ [values applicable to ZnS (see below and Refs. 47–54)], we obtain for $(\mathcal{E}_{\text{eff}}/\mathcal{E})^2b^2$ the value 4.2×10^{-6}. For the electric-dipole part, if we guess that $|\langle E\theta|R_z|T_2\zeta\rangle|$ might be 0.1 Å, then if $\bar{\nu}_0=3400$ cm^{-1} we obtain $a^2=5.5\times10^{-4}$.

The zeroth and first moments of the full ${}^5E\rightarrow{}^5T_2$ absorption curve provide a convenient means of determining the cubic-field parameter Dq apart from a small second-order spin-orbit correction. Setting $\alpha(\nu)=\nu g(\nu)$ in Eq. (4.9), we define the nth moment by

$$M_n=\int(h\nu)^n g(\nu)d\nu, \tag{4.20}$$

where the integral is over all components of ${}^5E\rightarrow{}^5T_2$. We then find from Table X (considering only the electric-dipole transitions) and the crystal-field energy levels[77] of ${}^5E$ and ${}^5T_2$ that for the low-temperature spectrum (when only the Γ_1 level of ${}^5E$ is appreciably occupied),

$$(M_1/M_0)_{T=0^\circ\text{K}}=10|Dq|+(672/25)\lambda^2/\Delta. \tag{4.21}$$

This value for the low-temperature moment ratio differs only slightly from the average energy of the ${}^5T_2$ states relative to the Γ_1 level of ${}^5E$,

$$\bar{E}({}^5T_2)-E(\Gamma_1;{}^5E)=10|Dq|+32\lambda^2/\Delta. \tag{4.22}$$

[77] The crystal-field energy levels of ${}^5E$ are as given in (4.1), while those of ${}^5T_2$ are given by (4.7) plus the energy displacement $10|Dq|+24\lambda^2/\Delta$ common to all the levels of ${}^5T_2$ and omitted from the relative energies given in (4.7).

B. Jahn-Teller Effects

The orbital degeneracy of both ${}^5E$ and ${}^5T_2$ in tetrahedral symmetry implies that both the initial and final states for the optical transition ${}^5E\rightarrow{}^5T_2$ are unstable with respect to nuclear displacements which lower the symmetry and lift the electronic degeneracy. This type of instability was first pointed out by Jahn and Teller,[23] and it leads to a coupling between the motion of the electrons and the vibrational motion of the lattice which can have a profound effect on the optical spectrum and other properties of the Fe^{2+} ion in a crystalline environment.[78]

The instability of the symmetrical nuclear configuration for an electronic state having orbital degeneracy implies the existence of several equivalent stable distorted configurations. A static distortion of the complex does not however actually occur unless the Jahn-Teller energy E_{JT} (the amount by which the energy of the entire system in a stable configuration is lower than that of the symmetrical configuration) is much greater than the zero-point energy of the associated modes of vibration. When this condition is not satisfied the vibrational motion of the complex even at 0°K is not localized about a single stable configuration, and the vibrations carry the system from the neighborhood of one such configuration to that of another while the electrons perform their corresponding coupled motion. This situation is termed the dynamical Jahn-Teller effect.

Since with a dynamical Jahn-Teller effect one does not have a static distortion, we shall classify the coupled vibronic states of the system by the irreducible representations of the symmetry group of the undistorted configuration (in our case T_d).[79] Vibronic states belonging as partners to the same irreducible representation then remain degenerate, since the coupled Hamiltonian retains the original symmetry. Accordingly, states of the coupled system (electrons and vibrations taken together) preserve their essential degeneracies (those arising from the multidimensionality of some of the irreducible representations of T_d) despite the Jahn-Teller coupling.

The spin-orbit levels of Fe^{2+} in a static tetrahedral crystal field have been described in the previous section. Each of these electronic states associates with the various vibrational states of the complex to give an infinite sequence of vibronic states. We observe optical

[78] References to the literature pertaining to the Jahn-Teller effect may be found in Ref. 24 and in a paper by Liehr [A. D. Liehr, J. Phys. Chem. **67**, 389 (1963)].

[79] In the limiting case of a static Jahn-Teller distortion it may be convenient first to classify states in terms of the symmetry of the *distorted* configurations. Linear combinations of corresponding states of the several equivalent distorted configurations then provide bases for the irreducible representations of the symmetry group of the *undistorted* configuration. When tunneling among the several distortions becomes important in the dynamic case, such states belonging to different irreducible representations of the latter become separated in energy in proportion to the tunneling frequency, while states transforming as partners under the same irreducible representation remain degenerate.

transitions from the lowest vibronic states derived from ^5E to the vibronic levels derived from $^5T_2$. Since the ground vibrational state of the complex (the state with no phonons present) transforms as $A_1(\Gamma_1)$ in the absence of the Jahn-Teller coupling, the vibronic state of lowest energy derived from each spin-orbit level of ^5E (4.1) or $^5T_2$ (4.7) belongs to the same Γ_n (since $\Gamma_n \times \Gamma_1 = \Gamma_n$), and we can follow these states continuously as the strength of the Jahn-Teller interaction is turned up. Levels belonging to different Γ_n may of course cross in energy, while those of the same Γ_n (including those derived from excited vibrational states) may mix but do not cross.

Obviously a detailed description of the vibronic levels is very complicated if the Jahn-Teller splitting ($\approx 3E_{JT}$), the spin-orbit splitting, and the phonon energies ($\hbar\omega$) are comparable, particularly if there are a number of important modes of vibrations.[80] However, the situation simplifies somewhat in certain situations which may be appropriate to tetrahedral iron, as we shall now describe.

If the Jahn-Teller splitting is appreciably larger than both the spin-orbit splitting and the phonon energies, it has been shown[24] that the Jahn-Teller coupling partially quenches the first-order spin-orbit interaction within the $^5T_2$ state, while it may either diminish or enhance the second order spin-orbit interactions within this state. The lowest group of vibronic levels derived from $^5T_2$ may still consist, however, of the same set of six levels (one Γ_1, one Γ_3, two Γ_4, and two Γ_5) obtained in the preceding section from the spin-orbit splitting of $^5T_2$ in crystal-field theory. This is the case, for example, when the predominant Jahn-Teller coupling with $^5T_2$ is with an E vibrational mode. When this is so, it was shown that a phenomenological Hamiltonian of precisely the same form as that introduced in Eq. (4.3) suffices to describe this lowest group of levels. The parameters ζ, μ, and ρ in this Hamiltonian are now no longer given by Eq. (4.8) but depend on the details of the Jahn-Teller interaction and the phonon frequencies as well as on the spin-orbit coupling. In particular, the first-order spin-orbit parameter ζ is diminished with respect to its value in Eq. (4.8) by a factor Q given approximately by

$$Q = \exp[-\xi(E_{JT}/\langle\hbar\omega\rangle)], \tag{4.23}$$

where $\langle\hbar\omega\rangle$ is an average energy for the effective phonons, and $\xi \approx \frac{3}{2}$. The second-order parameters μ and ρ may or may not be diminished with respect to their original values (4.8), but in addition they may be augmented by a further term of magnitude λ^2/E_{JT}.

Thus, despite a strong Jahn-Teller effect, a Hamiltonian of the form (4.3) may still be useful in describing the lowest vibronic states derived from $^5T_2$, but the parameters ζ, μ, and ρ may assume values very different from those one gets from spin-orbit splitting ignoring the Jahn-Teller effect. Optical transitions to this lowest group of vibronic levels of $^5T_2$ (from the lowest levels of ^5E) are the ones we refer to as zero-phonon transitions.

Alternatively, the lowest group of vibronic levels derived from $^5T_2$ may include additional states not comprised in the six spin-orbit levels of $^5T_2$ in crystal-field theory. Such additional states derive, in the limit of no Jahn-Teller coupling, from excited vibrational states, and one or more such states may be depressed in energy as the strength of the Jahn-Teller coupling increases, eventually mingling with the lowest group if the Jahn-Teller coupling is of suitable form. For example, if the Jahn-Teller coupling with $^5T_2$ is predominantly with a T_2 vibrational mode (corresponding to a limiting static distortion of [111] symmetry), two additional levels, one Γ_3 and one Γ_5, are brought down in energy in this fashion, so that with a strong Jahn-Teller coupling the lowest group derived from $^5T_2$ should consist of one Γ_1, two Γ_3, two Γ_4, and three Γ_5. In such a case, while Jahn-Teller quenching of the first-order spin-orbit interaction still occurs, the phenomenological Hamiltonian (4.3) must be augmented to describe the additional levels and their spin-orbit coupling to the original six.

We shall show in Sec. V that for Fe^{2+} in ZnS and possibly also in $MgAl_2O_4$ a phenomenological Hamiltonian of the form (4.3), with parameters reflecting the importance of Jahn-Teller coupling, may be used successfully to fit the level structure of $^5T_2$ as inferred from the experimental spectra. For Fe^{2+} in CdTe, however, we shall see that this description is insufficient to account for the data, and that one must suppose that additonal states are brought down in energy by the Jahn-Teller coupling

For the ^5E state the effect of Jahn-Teller coupling takes a quite simple form, provided we can assume that the Jahn-Teller interaction is at most only moderately strong, so that a static distortion does not occur and only the linear Jahn-Teller coupling need be considered.[81] The ^5E state is split only in second order by spin-orbit interactions, as given in (4.1) and (4.2). The over-all splitting $4K$ is consequently fairly small [$4K \lesssim 80$ cm^{-1} if $|\lambda| \lesssim 100$ cm^{-1}, $\Delta \approx 3000$ cm^{-1}] relative to the important phonon energies. Assuming Jahn-Teller coupling with a single E vibrational mode, we can then show (much as in Sec. III of Ref. 24) that the effect of the Jahn-Teller coupling on the second-order spin-orbit splitting (4.1) is given approximately

[80] Strictly, we should consider all the phonons of the lattice, but we may approximate their effect by appropriate oscillators with frequencies near the critical points in the lattice phonon spectrum, augmented if necessary by localized modes characteristic of the impurity ion and its immediate neighbors.

[81] For an E state, linear Jahn-Teller coupling can involve only E vibrational modes; one obtains a continuum of equivalent distorted configurations unless quadratic Jahn-Teller coupling or anharmonic terms are sufficiently strong to make a particular set of distortions stable. [See J. B. Goodenough, J. Phys. Chem. Solids **25**, 151 (1964).]

simply by replacing the crystal-field value of K by

$$K' \approx (\tfrac{1}{2})K\{1+\exp[-4E_{JT}(^5E)/\hbar\omega]\}. \quad (4.24)$$

Thus the dynamical Jahn-Teller effect acts in this approximation simply to diminish by perhaps as much as $\approx\frac{1}{2}$ the spacing of the spin-orbit levels (4.1), without changing the order of the levels or disturbing the uniformity of their spacing.

In addition to changing the energies of the vibronic levels, the Jahn-Teller coupling of course also changes the intensities of the optical transitions between ^5E and $^5T_2$. The zero-phonon line intensities are diminished, while transitions to excited vibronic states of the final state (that is, "phonon-assisted" transitions corresponding to the emission of one or more phonons) are enhanced. The rigorous selection rules for electric dipole or magnetic dipole transitions in tetrahedral symmetry are however still obeyed between the initial and final vibronic states. These selection rules were given in Table IX.

The over-all $^5E \rightarrow {}^5T_2$ optical spectrum is broadened by the Jahn-Teller effect because of the enhanced intensity of the phonon-assisted transitions. Nevertheless, if the Jahn-Teller interaction in the ^5E state is negligible (we show in Sec. V that it is weak for tetrahedral Fe^{2+} in the crystals studied here) then it can be proved that the moments M_0 and M_1, as defined in Eq. (4.20), of the full $^5E \rightarrow {}^5T_2$ spectrum, including the phonon-assisted lines, are not changed by linear Jahn-Teller coupling in the $^5T_2$ state.[82] M_0 and M_1 are also unaffected by differences between ^5E and $^5T_2$ in the linear coupling to symmetric modes of vibration. Accordingly, the total oscillator strength F_{tot} of the band still has the value given by Eq. (4.19). Moreover, we may continue to use the ratio (M_1/M_0) of the low-temperature spectrum to obtain to a good approximation, from Eq. (4.21), the electronic cubic-field-splitting parameter Dq (apart from the small second-order spin-orbit correction).[83]

The Jahn-Teller coupling lowers the average energy of the lowest group of vibronic levels of $^5T_2$ (the final states for the zero-phonon transitions) by approximately the Jahn-Teller energy $E_{JT}(^5T_2)$ (neglecting spin-orbit corrections). Accordingly an approximate value for $E_{JT}(^5T_2)$ is given by the difference between the average energy of these states, as obtained from the zero-phonon lines, and the original unshifted average electronic energy of the $^5T_2$ state as obtained from the moment ratio $(M_1/M_0)_{T=0°K}$ and Eqs. (4.21) and (4.22). The value of $E_{JT}(^5T_2)$ so obtained will, however, be somewhat larger than the true value, since the lowest group of states is lowered not only by the Jahn-Teller coupling but also by any difference between ^5E and $^5T_2$ in the coupling of these states to symmetric vibrational modes.[84]

Although the total oscillator strength F_{tot} may be unaffected by the Jahn-Teller coupling of $^5T_2$, the sum F_0 of the oscillator strengths of the zero-phonon lines is of course diminished. Under the assumption that Jahn-Teller effects in the ^5E state are small enough to be ignored, we have approximately,[85] at 0°K,

$$(F_0/F_{tot})_{0°K} \approx \exp[-E_{JT}(^5T_2)/\langle\hbar\omega\rangle], \quad (4.25)$$

[82] This proof can be given using methods similar to those of C. H. Henry, S. E. Schnatterly, and C. P. Slichter, Phys. Rev. **137**, A583 (1965). The proof applies to an allowed transition (either electric- or magnetic-dipole) and requires that mixing of the initial and final states, via electron-lattice or spin-orbit interactions, either with each other or with other states, be negligible (thus, that there is negligible "borrowing" of intensity from other transitions). It also requires, as noted, that Jahn-Teller coupling in the initial state be negligible.

[83] The value of Dq so obtained reflects not only the cubic field matrix element of simple crystal-field theory, but also the contribution of covalent bonding, etc., to the electronic energy difference, as well as any difference in lattice zero-point energy between $^5T_2$ and ^5E.

[84] It has been customary, following the work of Orgel [L. E. Orgel, J. Chem. Phys. **23**, 1824 (1955)], to assume that the band widths in the optical spectra of transition metal complexes arise principally, via the dependence of the energy of the transition on Dq, from the difference in the coupling of the initial and final electronic states to a symmetric mode of vibration of the nearest neighbors. The additional broadening due to Jahn-Teller coupling to nonsymmetric modes is usually assumed to be of less importance. In contrast, the point of view taken in this paper is that for the spectra considered here the Jahn-Teller coupling is responsible for a major part of this broadening (or equivalently, for a major fraction of the empirical value for $E_{JT}(^5T_2)$ obtained, as described in the text, from the observed spectra). The difference, we suggest, is related to the fact that $|Dq|$ is so much smaller for the tetrahedral ions studied here than for the complexes considered by Orgel and others. Crystal-field theory gives the relation that the derivative of Dq with respect to the local dilatation $\theta(=e_{11}+e_{22}+e_{33}$ in terms of the local strain) is simply

$$\frac{\partial(Dq)}{\partial\theta} = -5/3(Dq)$$

(of course, so simple a relation can hold only approximately, if at all, in an actual situation in which overlap and covalency are important). The contribution of the symmetrical mode of vibration to the broadening is proportional to the square of this derivative. Thus if Dq is small, this contribution to the empirical value of $E_{JT}(^5T_2)$ may be very much diminished in proportion to $(Dq)^2$.

[85] This result may be derived rigorously for the model for $^5T_2$ used in Sec. II, Ref. 24 (it is really for the fraction of M_0, rather than M_1, associated with the zero-phonon lines that Eq. (4.25) is true in this case; however so long as $E_{JT} \ll 10|Dq|$ the relation holds to a very good approximation for M_1 as well). The relation is correct also for the reduction in F_0 arising from any difference between ^5E and $^5T_2$ in their linear coupling to symmetric vibrational modes, if in Eq. (4.25) E_{JT} in this case is replaced by the energy by which the lowest vibronic level of $^5T_2$ is lowered relative to that of ^5E by this difference. When several independent vibrational modes are active, the exponent in Eq. (4.25) should equal the sum of the ratios $(E_{JT}/\hbar\omega)_i$ for each mode, and the average value $\langle\hbar\omega\rangle$ in Eq. (4.25) is to be taken in this sense. In more complicated cases of a Jahn-Teller effect (for example, that of Sec. III, Ref. 24) Eq. (4.25) has not been shown to hold, although it must be roughly correct. The expression (4.25) is the analog of the expression for the intensity of the Mössbauer line (at 0°K) in the theory of the Mössbauer effect, except that of course for the latter the recoil energy R of the free ion replaces E_{JT} in the exponent [R. L. Mössbauer, Z. Physik **151**, 124 (1958); W. E. Lamb, Jr., Phys. Rev. **55**, 190 (1939); W. M. Visscher, Ann. Phys. (N.Y.) **9**, 194 (1960); H. J. Lipkin, Ann. Phys. (N.Y.) **9**, 332 (1960); see also H. Frauenfelder, *The Mössbauer Effect* (W. A. Benjamin, Inc., New York, 1962), Chap. 2]. Such expressions (or ones equivalent) for the intensity of zero-phonon lines in optical spectra are familiar, at least for the case of nondegenerate electronic states interacting with totally symmetric vibrational modes, from the work of many authors {see for example K. Huang and A. Rhys, Proc. Roy. Soc. (London) **A204**, 406 (1950); E. O. Kane, Phys. Rev. **119**, 40 (1960); E. D. Trifonov, Dokl. Akad. Nauk SSSR **147**, 826 (1962) [English transl.: Soviet Phys.—Doklady **7**, 1105 (1963)]}.

TABLE XI. Relative oscillator strengths $f_e(A,B)/a'^2$ and $f_m(A,B)/b'^2$ for electric- and magnetic-dipole transitions between the lowest groups of vibronic spin-orbit levels of ^5E and $^5T_2$.[a]

Initial level A of ^5E		Final level B of $^5T_2$					
Electric-dipole transition	Magnetic-dipole transition	$\Gamma_5(-)$	$\Gamma_4(-)$	$\Gamma_5(+)$	$\Gamma_4(+)$	Γ_3	Γ_1
(No. 1) Γ_1	(No. 5) Γ_2	$\frac{1}{2}(1-x)$	0	$\frac{1}{2}(1+x)$	0	0	0
(No. 2) Γ_4	(No. 4) Γ_5	$\frac{1}{4}(1+x)$	$\frac{1}{4}(1-y)$	$\frac{1}{4}(1-x)$	$\frac{1}{4}(1+y)$	0	0
(No. 3) Γ_3	(No. 3) Γ_3	$\frac{1}{4}(1-x)$	$\frac{1}{4}(1+y)$	$\frac{1}{4}(1+x)$	$\frac{1}{4}(1-y)$	0	0
(No. 4) Γ_5	(No. 2) Γ_4	$\frac{1}{12}(1+x)$	$\frac{1}{12}(1-y)$	$\frac{1}{12}(1-x)$	$\frac{1}{12}(1+y)$	4/9	2/9
(No. 5) Γ_2	(No. 1) Γ_1	0	$\frac{1}{2}(1+y)$	0	$\frac{1}{2}(1-y)$	0	0

[a] The values given in the table for $f_e(A,B)/a'^2$ and $f_m(A,B)/b'^2$ have been summed over the degenerate states of the final vibronic spin-orbit level B and averaged over those of the initial level A. The parameters x and y are defined in Eqs. (4.28) and (4.29) of the text, the quantities a'^2 and b'^2 by Eqs. (4.26) and (4.27) (the latter for the case of a negligible Jahn-Teller coupling in ^5E). The states of $^5T_2$ used in this table are the eigenstates of the phenomenological Hamiltonian (4.3), which includes the effects of Jahn-Teller coupling. The states of ^5E are as given in (4.1).

where $\langle\hbar\omega\rangle$ is an average energy for the effective phonons.

The oscillator strengths of individual zero-phonon lines, taking account of the Jahn-Teller coupling of $^5T_2$, may be obtained from Table XI if the Hamiltonian (4.3) gives a good description of the lowest group of vibronic levels of $^5T_2$. The parameters $(a')^2$ and $(b')^2$ in Table XI are given by

$$(a')^2 \approx a^2 \exp[-E_{JT}(^5T_2)/\langle\hbar\omega\rangle], \quad (4.26)$$

$$(b')^2 \approx b^2 \exp[-E_{JT}(^5T_2)/\langle\hbar\omega\rangle] \quad (4.27)$$

in accordance with Eq. (4.25), where a^2 and b^2 were defined by Eqs. (4.15) and (4.16), while x and y are defined in terms of the phenomenological parameters ζ, μ, and ρ of (4.3) by

$$x=(\rho+\zeta-\mu)/\Delta E(\Gamma_5), \quad (4.28)$$

$$y=(3\rho+\zeta+\mu)/\Delta E(\Gamma_4). \quad (4.29)$$

Here

$$\Delta E(\Gamma_5)=[(\rho+\zeta-\mu)^2+24(\zeta-\mu)^2]^{1/2} \quad (4.30)$$

is the energy difference between the pair of eigenstates of (4.3) belonging to Γ_5, and

$$\Delta E(\Gamma_4)=[(3\rho+\zeta+\mu)^2+8(\zeta+\mu)^2]^{1/2} \quad (4.31)$$

is the energy difference of the Γ_4 pair. Since with the Jahn-Teller coupling we can no longer assume $|\zeta|\gg|\rho|$, we must now replace the approximate values given in (4.7) for the Γ_4 and Γ_5 energies by their exact values obtained by solving the secular equation of (4.3) for each pair,

$$E_\pm(\Gamma_4)=\tfrac{1}{2}\{\zeta+5\mu+7\rho\pm\Delta E(\Gamma_4)\}, \quad (4.32)$$

$$E_\pm(\Gamma_5)=\tfrac{1}{2}\{-\zeta+13\mu+11\rho\pm\Delta E(\Gamma_5)\}. \quad (4.33)$$

The energies for Γ_1 and Γ_3 given in (4.7) are already exact eigenvalues of (4.3).

V. COMPARISON OF EXPERIMENTAL RESULTS WITH THEORY

In this section we shall compare the observed Fe^{2+} spectra in ZnS, CdTe, and $MgAl_2O_4$ with the theory given in Sec. IV, in order to ascertain values for as many as possible of the parameters that determine the energy-level structure of tetrahedral Fe^{2+} in these crystals.

It is immediately clear from a quick comparison of the observed low-temperature spectra with the static crystal-field model that this model as applied to the $^5T_2$ state completely fails to account for most of the structure that we have ascribed to zero-phonon transitions, at least if the spin-orbit parameter λ has a value even remotely approximated by its free-ion value ≈ -100 cm^{-1}. In particular, at the lowest temperature when all the Fe^{2+} should be in the Γ_1 level of ^5E, we find from (4.7), Fig. 10, and Table IX, assuming an electric-dipole transition, that the zero-phonon spectrum should consist of only two strong lines separated by $\approx 5|\lambda|$, the lower of which is the transition to the lowest level of $^5T_2$ [the Γ_5 level with $J'=1$ in (4.7) and Fig. 10]. We would expect the separation between these two lines to be at least ≈ 350 cm^{-1}, assuming that covalent and overlap effects reduce $|\lambda|$ in the crystal to no less than some 70% of its free ion value. Since the second lowest level of $^5T_2$ [the Γ_4 level with $J'=2$ in (4.7) and Fig. 10] lies $\approx 2|\lambda|$ above the lowest, according to crystal-field theory no zero-phonon lines arising from transitions to the higher levels of $^5T_2$ should lie within ≈ 140 cm^{-1} of the lower strong line, even if these other transitions are allowed by other transition mechanisms (e.g., magnetic-dipole processes). In contrast, the low-energy end of the observed spectrum of Fe^{2+} in ZnS at 2.7°K (Fig. 3) shows three zero-phonon lines (the higher two weak) within a range of 40 cm^{-1}. Fe^{2+} in CdTe at 3.5°K (Fig. 7) shows three moderately strong lines within a range of 30 cm^{-1}, and at least two weaker lines at slightly higher energy. And the $MgAl_2O_4$ spectrum at 6.9°K (Fig. 9) shows two strong lines separated by 65 cm^{-1}, and at least one weaker zero-phonon line at higher energy.

Accordingly, we must either suppose that most of the observed structure does not in fact arise from tetrahedral Fe^{2+} [a possibility which we incline to discount.

since the lines of principal interest appear with the same relative intensity in different samples having quite different iron concentrations (see Table I)], or else adopt a drastically altered model. We take the latter course, invoking dynamical Jahn-Teller effects in the $^5T_2$ state to account for the marked departures from the crystal-field model. The importance of such effects will be given quantitative justification below.

For the ^5E state, on the other hand, the crystal-field model will be shown to describe the levels quite well, Jahn-Teller effects evidently being of no great importance in this state.

A. Cubic-Field Parameter, Dq

The only absorption band in ZnS, CdTe, and $MgAl_2O_4$ which we have been able to attribute with confidence to the presence of Fe^{2+} has its center at 3500, 2700, and 4600 cm^{-1}, respectively, for a temperature of 300°K. The position of the band is similar to the value 2800 cm^{-1} obtained for this transition for Fe^{2+} in CdS by Pappalardo and Dietz.[7]

Quite precise values for Dq for tetrahedral Fe^{2+} in these crystals may be obtained, using Eq. (4.21), if we evaluate the moment ratio (M_1/M_0) of this absorption band at a temperature sufficiently low that only the lowest level of ^5E is appreciably populated. We have obtained for this ratio the values 3470±5 2530±5, and 4530±5 cm^{-1} for ZnS (2.7°K, Fig. 3), CdTe (3.5°K, Fig. 7), and $MgAl_2O_4$ (6.9°K, Fig. 9), respectively. Making the small correction for the second order spin-orbit term in Eq. (4.21) (using a value for λ^2/Δ obtained from the observed separation of the levels of ^5E), we obtain therefore the values

$$|Dq| = 340, \quad 248, \quad 447 \text{ cm}^{-1} \tag{5.1}$$

for ZnS, CdTe, and $MgAl_2O_4$, respectively. Since $^5T_2$ lies higher than ^5E, Dq is negative.

The value $Dq = -447$ cm^{-1} for Fe^{2+} in $MgAl_2O_4$ given in (5.1) agrees with the prediction of the simple crystal-field theory that in tetraherdal coordination Dq should have a value approximately 4/9 (and of the opposite sign) of its value for the corresponding octahedral environment. For octahedral oxide coordination McClure[70] gives $Dq \approx +1000$ cm^{-1} for Fe^{2+}. A value similar to that for Fe^{2+}, namely $Dq = -400$ cm^{-1}, was cited by Weakliem[11] for Co^{2+} in tetrahedral coordination in $MgAl_2O_4$ from unpublished work by McClure. In another tetrahedrally coordinated oxide, the values −390, −420, and −500 cm^{-1} have been obtained by Weakliem[11] for Co^{2+}, Ni^{2+}, and Cu^{2+}, respectively, in ZnO. Pappalardo *et al.*[6,8,9] have obtained −390, −405, and −480 cm^{-1} for Co^{2+}, Ni^{2+}, and Cu^{2+}, respectively, in ZnO.

The appreciably smaller value $Dq = -340$ cm^{-1} obtained in (5.1) for Fe^{2+} in ZnS is similar to values obtained by Weakliem[11] and by Pappalardo and Dietz[7] for Co^{2+} in ZnS and CdS. The midpoint of the Fe^{2+} absorption band in cubic ZnS at 300°K as found by Coblentz[1] and by Low and Weger[3] both give a Dq of -330 cm^{-1}.

The value $|Dq| = 248$ cm^{-1} for Fe^{2+} in CdTe is somewhat smaller than that one would infer for Fe^{2+} in CdS from the data of Pappalardo and Dietz,[7] and it is one of the smallest values ever attributed to a cubic-field parameter for a transition metal of the iron group. Values of Dq for other transition metal ions in CdTe, or for other tellurides, have not yet been obtained from optical measurements. Values that may be estimated from available g shifts[71] are not reliable so long as one does not know the proper value of the effective spin-orbit parameter in these crystals.

B. Total Oscillator Strength, F_{tot}

From the values for the total oscillator strength of the full $^5E \rightarrow {}^5T_2$ band given in Table VI, we get in accordance with Eq. (4.19) the following values for the parameter a^2 of Eq. (4.15) [using the 0°K values for F_{tot}, assuming that the conditions noted in Sec. IVB for the invariance of F_{tot} are approximately satisfied, and ignoring b^2 in Eq. (4.19) since b^2 contributes at most less than 1% of F_{tot}]

$$a^2 = 6.4\times10^{-4}, \ 1.8\times10^{-4}, \ 5.0\times10^{-4} \tag{5.2}$$

for ZnS, CdTe, and $MgAl_2O_4$, respectively. These values correspond respectively, with use of Eq. (4.15), to the following values (in angstroms) for the matrix element $|\langle E\theta|R_z|T_z\zeta\rangle|$: 0.11, 0.07, 0.08. The latter are a measure of the effect of the odd part of the static tetrahedral crystal field in mixing states of odd parity into the ^5E and $^5T_2$ states of the Fe^{2+} ion and thereby making the $^5E \rightarrow {}^5T_2$ transition electric-dipole allowed. Since the measured values for F_{tot} increase only a little as the temperature is raised from 0° to 300°K (Table VI), it is clear that the static part of the crystal field (including the effect of covalent bonding) in these crystals is much more important than the lattice vibrations in making this transition allowed, in agreement with the assumptions made in Sec. IV.

C. Levels of ^5E

The five spin-orbit levels of ^5E are given by crystal-field theory to be disposed as in (4.1) and Fig. 10, with the singlet Γ_1 lowest, and to be approximately equally spaced with a separation $K = 6\lambda^2/\Delta$ as in Eq. (4.2). As described in Sec. IVB, dynamical Jahn-Teller effects may diminish this separation somewhat but should not alter either the order of the levels or the uniformity of the spacing. The experimental results conform quite well to this prediction. As inferred from the frequencies of the lines (1-6), (2-6), (3-6), and (4-6) [and also (5-6) for ZnS] in Table II, the levels are consistent within experimental accuracy with a

uniform separation

$$K=15\pm2\ \text{cm}^{-1},\ 10\pm2\ \text{cm}^{-1},\ 13\pm2\ \text{cm}^{-1} \quad (5.3)$$

for ZnS, CdTe, and $MgAl_2O_4$, respectively (Table III). Equating K to $6\lambda^2/\Delta$ as in Eq. (4.2), and using the values of $\Delta=10|Dq|$ from (5.1), we obtain for the effective spin-orbit parameter connecting ^5E and $^5T_2$ states of Fe^{2+} in these crystals the values

$$|\lambda|=92\pm10\ \text{cm}^{-1},\ 64\pm10\ \text{cm}^{-1},\ \text{and}\ 98\pm10\ \text{cm}^{-1}, \quad (5.4)$$

respectively. The first and third of these, for ZnS and $MgAl_2O_4$, agree within the indicated uncertainty with the free-ion value[72] $\lambda\approx-100\pm10$ cm^{-1} for Fe^{2+}, while the smaller value of $|\lambda|$ for Fe^{2+} in CdTe can quite plausibly be attributed to the effects of covalent bond-bonding and overlap. Assuming that Jahn-Teller effects should be of somewhat similar importance in all three crystals, we conclude from these results that Jahn-Teller effects are not pronounced in the ^5E state of Fe^{2+} in these crystals and that crystal-field theory gives a good description of this state. A small Jahn-Teller energy for the ^5E state of tetrahedral Fe^{2+} is consistent with the fact that the relevant distortion involves only shearing motions of the four nearest neighbors which to first order leave unchanged the Fe^{2+}-nearest-neighbor distance, and may therefore couple but weakly to the e electron on the Fe^{2+}.

Only for Fe^{2+} in ZnS is the line (5-6) observed, so that for CdTe and $MgAl_2O_4$ we have no experimental evidence giving the energy of level No. 5, the highest of the ^5E levels. The transition $\Gamma_2\rightarrow\Gamma_5$ is electric-dipole forbidden, so that the line (5-6) should be absent unless level No. 6 comprises a Γ_4 state as well as Γ_5, as we believe to be the case for ZnS (see below). We presume from the theoretical model that level No. 5 lies one interval K higher than No. 4 in all three crystals, and this is confirmed for ZnS. Unfortunately, at temperatures at which level No. 5 should be appreciably populated the absorption lines to levels above the lowest level (No. 6) of $^5T_2$ have become too broad to permit us to resolve any other transition originating in No. 5.

D. Levels of $^5T_2$

The crystal-field model, as noted previously, fails to account for the energy levels of $^5T_2$ (Table III) as inferred from the zero-phonon lines of the observed low-temperature spectrum. This failure we ascribe to dynamical Jahn-Teller effects, the importance of which in the $^5T_2$ state of tetrahedral Fe^{2+} we now wish to justify.

We may estimate the Jahn-Teller energy of the $^5T_2$ state, $E_{JT}(^5T_2)$, as noted in Sec. IVB, from the difference between the average electronic energy (4.22) of $^5T_2$ (relative to Γ_1 of ^5E), as inferred from the moment ratio (M_1/M_0), and the average energy of the lowest vibronic levels of $^5T_2$, as obtained from the zero-phonon lines. Using as an approximation to the latter the energy of the line (1-6), we obtain from the values of (M_1/M_0) cited in connection with the evaluation of Dq the following values

$$E_{JT}(^5T_2)\approx535\ \text{cm}^{-1},\ 255\ \text{cm}^{-1},\ 945\ \text{cm}^{-1} \quad (5.5)$$

for ZnS, CdTe, and $MgAl_2O_4$, respectively. These values provide an upper bound to the correct value of $E_{JT}(^5T_2)$ for Fe^{2+} in these crystals; apart from the small spin-orbit correction to (5.5) the principal source of uncertainty is that we have no clear way at present to distinguish what fraction of (5.5) is the true Jahn-Teller energy, and what fraction the lowering of the vibronic levels due to the difference between ^5E and $^5T_2$ in their linear coupling to symmetric modes of vibration.[86]

The fraction (F_0/F_{tot}) of the total oscillator strength of the $^5E\rightarrow{}^5T_2$ absorption band which is represented by the zero-phonon lines at 0°K was given in Eq. (4.25) and provides a value for the ratio $E_{JT}(^5T_2)/\langle\hbar\omega\rangle$. Here $\langle\hbar\omega\rangle$ is an average energy for the effective phonons, and the appropriate value for E_{JT} to be used in this ratio should include the effect of symmetric modes in lowering the vibronic levels, as noted earlier. The values for this ratio obtained from the experimental values for (F_0/F_{tot}) near 0°K (Table VI) are

$$E_{JT}(^5T_2)/\langle\hbar\omega\rangle=2.5,\ 1.8,\ 1.9 \quad (5.6)$$

for ZnS, CdTe, and $MgAl_2O_4$, respectively. We may use these values together with (5.5) to obtain the following average energies for the effective phonons in these crystals:

$$\langle\hbar\omega\rangle=215\ \text{cm}^{-1},\ 140\ \text{cm}^{-1},\ 495\ \text{cm}^{-1}. \quad (5.7)$$

These values for $\langle\hbar\omega\rangle$ are very reasonable, being in each case higher than the energies of the TA and LA phonons but lower than those of TO and LO (Tables V, VII, and VIII).

The Jahn-Teller quenching of the first-order spin-orbit interaction in $^5T_2$ is given by the quenching factor Q, Eq. (4.23), which like (F_0/F_{tot}) depends exponentially on the ratio $E_{JT}(^5T_2)/\langle\hbar\omega\rangle$. However, symmetric modes of vibration do not contribute to this quenching, so that in evaluating Eq. (4.23) we should use the true Jahn-Teller energy in forming this ratio. Accordingly, the value for this ratio appropriate to Eq. (4.23) should be somewhat smaller than the value (5.6) obtained from (F_0/F_{tot}). Using (5.6) to evaluate Eq. (4.23) (using $\xi=1.5$), we therefore obtain the following lower

[86] We may estimate this latter fraction if we accept the relation given in Ref. 84 relating the change in Dq with dilatation to Dq itself. Using the values for Dq given in (5.1), we may then calculate that in each case only some 10 to 15% of the empirical value for $E_{JT}(^5T_2)$ given in (5.5) is contributed by the symmetric mode. Clearly, it would be desirable for $\partial(Dq)/\partial\theta$ to be determined experimentally, as one could do by measuring the change of frequency of the zero-phonon lines with compression, in order to check this estimate.

bounds for Q:

$$Q=0.023,\ 0.06,\ 0.06 \tag{5.8}$$

for ZnS, CdTe, and $MgAl_2O_4$, respectively.

If, therefore, the true Jahn-Teller energy makes up a substantial part of the values (5.5) and (5.6), we see from (5.8) that we can expect a strong quenching of the spin-orbit interaction in $^5T_2$, and, consequently, a much smaller over-all separation of the spin-orbit levels of $^5T_2$ than predicted by crystal-field theory. This indeed is what the experimental spectra show in all three crystals. Accordingly, if the phenomenological Hamiltonian (4.3) serves to describe the lowest group of vibronic levels derived from $^5T_2$, we may expect that the first-order spin-orbit parameter ζ will be much smaller than the free-ion value λ and perhaps of nearly the same magnitude as the second-order parameters μ and ρ. We now examine each case to see to what extent such a model can be used successfully to fit the experimental spectra, and to what extent it must be augmented to include additional levels.

Of the six lowest vibronic levels of $^5T_2$ described by the Hamiltonian (4.3), only the two with energies given by Eq. (4.33) belong to Γ_5, and it is to these levels only that the selection rules (Table IX) allow electric-dipole transitions from a Γ_1 initial state. When at the lowest temperatures only the Γ_1 state of ^5E is appreciably populated, the optical spectrum should therefore show only two strong zero-phonon lines separated in energy by $\Delta E(\Gamma_5)$ [Eq. (4.30)] if (4.3) is applicable (or possibly only one strong line if x in Table XI is near $+1$ or -1). The oscillator strengths of these two lines are then given by the first row of Table XI.

The low temperature spectra of Fe^{2+} in ZnS (Fig. 3), CdTe (Fig. 7), and $MgAl_2O_4$ (Fig. 9) show, respectively, one, three, and two strong zero-phonon lines. It is therefore evident that the Hamiltonian (4.3) may be applicable for Fe^{2+} in ZnS and $MgAl_2O_4$, but that it will not suffice for CdTe. We now consider each of these cases in detail.

Fe^{2+} in ZnS

We have found that the zero-phonon spectrum of Fe^{2+} in ZnS can be accounted for on the basis of the Hamiltonian (4.3), using the following values for the parameters,

$$\begin{aligned}\zeta&=+3.0\ \text{cm}^{-1},\\ \mu&=+4.5\ \text{cm}^{-1},\\ \rho&=-14.0\ \text{cm}^{-1}.\end{aligned} \tag{5.9}$$

From these, we obtain the values

$$\begin{aligned}x&=-0.90,\\ y&=-0.85\end{aligned} \tag{5.10}$$

for the parameters in Eqs. (4.28) and (4.29) and Table XI which give the relative oscillator strengths of the lines. For the relative energies of the levels of $^5T_2$ we obtain the values given in Table XII, where $\Gamma_5(-)$, $\Gamma_5(+)$ denote, respectively, the lower and upper levels of the pair belonging to Γ_5, and similarly for Γ_4. We identify the single strong line (1-6) of the experimental low-temperature spectrum with the transition $\Gamma_1\rightarrow\Gamma_5(-)$. The separation of $\Gamma_5(+)$ from $\Gamma_5(-)$ in Table XII then agrees with that of levels No. 6 and No. 7 in Table III, and we identify level No 7 with $\Gamma_5(+)$ and line (1-7) with $\Gamma_1\rightarrow\Gamma_5(+)$. This line is found to have an oscillator strength only 1/40 of that of (1-6), in agreement (to within the experimental uncertainty) with the ratio 1/20 obtained from the value $x=-0.90$ of (5.10). The energy by which $\Gamma_4(+)$ lies above $\Gamma_5(-)$ in Table XII agrees with the separation of levels No. 6 and No. 8 in Table III, and we therefore identify level No. 8 with $\Gamma_4(+)$, and the third line of the low-temperature spectrum, (1-8), with $\Gamma_1\rightarrow\Gamma_4(+)$. This transition is electric-dipole–forbidden in perfect tetrahedral symmetry, and the line (1-8) is somewhat too strong ($f\approx 5\times10^{-7}$ to within a factor of 2) to be reconciled with the value predicted[87] ($f\approx5\times10^{-8}$) on the basis of a magnetic-dipole transition. However, in the presence of random strains the transition $\Gamma_1\rightarrow\Gamma_4(+)$ becomes electric-dipole allowed because such strains mix the $\Gamma_5(-)$ and $\Gamma_4(+)$ states of $^5T_2$ (and also the Γ_1 and Γ_3 states of ^5E). A calculation leads to the conclusion that the observed oscillator strength of (1-8) [$\approx1\%$ of that of (1-6)] can be reconciled easily with the low-temperature linewidth ($\approx$4-7 cm^{-1}) of (1-6) (due also to strains) if (1-8) is indeed the $\Gamma_1\rightarrow\Gamma_4(+)$ transition. The other levels in Table XII, namely $\Gamma_4(-)$, Γ_3, and Γ_1, do not correspond to any of the observed levels identified in Table III. However, $\Gamma_4(-)$ as given in Table XII is too close to $\Gamma_5(-)$ to have permitted the $\Gamma_1\rightarrow\Gamma_4(-)$ line to have been resolved (moreover, it should be extremely weak, since according to Table XI it is very weakly allowed even for a magnetic-dipole transition), while the transitions $\Gamma_1\rightarrow\Gamma_3$ and $\Gamma_1\rightarrow\Gamma_1$ are forbidden both as electric- and magnetic-dipole processes. The model for $^5T_2$ based on the set of parameters (5.9) is thus consistent with the separation and

TABLE XII. Energy levels of $^5T_2$ for Fe^{2+} in ZnS, as calculated from the phenomenological Hamiltonian of Eq. (4.3) using the set of parameters given in (5.9).

State	Energy[a] (cm^{-1})
$\Gamma_5(-)$	0
$\Gamma_4(-)$	+ 1.3
$\Gamma_5(+)$	+17.2
Γ_3	+31.3
$\Gamma_4(+)$	+41.8
Γ_1	+53.8

[a] Energies are given relative to the lowest level, $\Gamma_5(-)$.

[87] We calculate an oscillator strength $f\approx5\times10^{-8}$ for $\Gamma_1\rightarrow\Gamma_4(+)$ on the basis of a magnetic-dipole transition if we use in Table XI the values $(\varepsilon_{\text{eff}}/\varepsilon)^2b^2\approx4.2\times10^{-6}$ [obtained from Eq. (4.16) using $\bar{\nu}_0=3400$ cm^{-1}, and $n^2=5.1$], $(b')^2/b^2=0.08$, $y=-0.85$, and $(\varepsilon_{\text{eff}}/\varepsilon)^2=[(n^2+2)/3]^2=5.6$.

TABLE XIII. Relative integrated intensity of zero-phonon lines of Fe^{2+} in ZnS at 33°K.

Transition	Theory[a]	Experiment
(1-6)	1.00	1.00
(2-6)	0.79	0.82
(3-6)	0.29	0.33
(4-6)	0.07	0.10
(5-6)	0.006	0.01

[a] The theoretical values are obtained from the model based on the Hamiltonian (4.3) and the parameters given by (5.9) and (5.10) (see text and Ref. 88).

relative strengths of the observed zero-phonon lines (and with the absence of other zero-phonon lines) at the low temperatures at which only the Γ_1 level of ^5E is occupied.

This model also accounts for the zero-phonon lines which appear at higher temperature and have levels No. 2–No. 5 of ^5E as initial states. We consider first the lines (2-6), (3-6), (4-6), and (5-6) which should appear, evenly spaced in accordance with (4.1), on the low-energy side of (1-6). We see from Table XII that the second level of $^5T_2$, $\Gamma_4(-)$, is placed only 1.3 cm^{-1} above $\Gamma_5(-)$. Since the minimum linewidth achieved in these experiments was ≈ 4 cm^{-1}, transitions to $\Gamma_5(-)$ and $\Gamma_4(-)$ are therefore not distinct, and oscillator strengths for these transitions must be combined for comparison with the experimental values. Although $\Gamma_4(-)$ contributes negligibly to the oscillator strength of (1-6), since $\Gamma_1 \rightarrow \Gamma_4(-)$ is electric-dipole–forbidden, we see from Table XI that this contribution is important for the lines (2-6), (3-6), (4-6), and (5-6). In particular, since $\Gamma_2 \rightarrow \Gamma_5(-)$ is electric-dipole forbidden, we should not expect to see the line (5-6) if level No. 6 did not comprise $\Gamma_4(-)$ as well as $\Gamma_5(-)$, while (2-6) would be weak (since x is near -1) instead of strong, as observed. Combining these oscillator strengths from Table XI, and multiplying by the appropriate degeneracy and Boltzmann factors for the initial states, we obtain the predicted relative intensities of the lines (1-6) through (5-6) as given in the second column of Table XIII for 33°K.[88] These agree satisfactorily with the experimental values at this temperature, given in the third column, which must be considered uncertain by possibly as much as a factor of 2 for the weaker lines.

The fact that no prominent additional zero-phonon lines are found to appear on the high-frequency side of (1-6) as the temperature is raised is also consistent with this model. From Table XI, we find that the line (2-7) [$\Gamma_4 \rightarrow \Gamma_5(+)$] should in fact be of comparable intensity to (2-6); however since the separation of levels 6 and 7 (19 ± 2 cm^{-1}) is the same as that of 1 and 2 (15 ± 2 cm^{-1}) to within the linewidth of (1-6), we conclude that the line (2-7) should be obscured by (1-6). The apparent oscillator strength of (1-6) is indeed found to increase somewhat with temperature, from 50×10^{-6} at 2.7°K to 80×10^{-6} at 33°K, although the uncertainties in these values are large enough to make this determination inconclusive. The other line originating in level No. 2 is the one corresponding to $\Gamma_4 \rightarrow \Gamma_4(+)$, but this line should be only about one-tenth as strong as (2-6), and it should moreover be broadened, since $\Gamma_4(+)$ can decay by phonon emission to $\Gamma_5(-)$, as well as being obscured by (1-7). Similarly, the transition $\Gamma_3 \rightarrow \Gamma_4(+)$ should be as strong as (3-6), but it is similarly broadened as well as being obscured in falling between (1-6) and (1-7). Other lines originating as levels No. 4 and No. 5 should be weak at low temperatures because of the low population of these levels, and at higher temperatures these lines should be both obscured by others and broadened.

The value $\zeta = +3.0$ cm^{-1} in (5.9) for the first-order spin-orbit parameter agrees rather well with the value $\zeta \approx 2.4$ cm^{-1} that one obtains by multiplying the crystal-field value (4.8) for ζ (using $\lambda \approx -100$ cm^{-1}) by the lower bound obtained in (5.8) for the quenching factor Q. The level structure of $^5T_2$ inferred from the experimental spectrum is thus consistent with our expectation that dynamical Jahn-Teller effects for Fe^{2+} in ZnS should produce a substantial quenching of the spin-orbit interaction within $^5T_2$. Moreover, as the quenching of ζ is almost as great as expected on the basis of the value (5.8) for the lower bound for Q, it appears that the values (5.5) and (5.6) in the case of Fe^{2+} in ZnS are for the most part accounted for by the *true* Jahn-Teller energy, and that the contribution of symmetric modes of vibration to the apparent E_{JT} is relatively small, in agreement with our estimate.[86]

The values (5.9) for the second-order spin-orbit parameters μ and ρ are quite close to $+K/3$ and $-K$, respectively, where K is the parameter (4.2) obtained from the observed separation of the levels of ^5E. Just such relations would be expected on the basis of crystal-field theory, using Eqs. (4.2) and (4.8), but it is surprising that they should still hold for Fe^{2+} in ZnS despite the strong quenching of ζ.[89]

The choice (5.9) for the parameters of our phenomenological model for $^5T_2$, using the Hamiltonian (4.3), cannot be changed significantly while preserving the indicated agreement with the experimental spec-

[88] The predicted relative intensities of Table XIII ignore contributions from transitions to higher levels of $^5T_2$ which give lines that overlap lines (1-6) through (5-6). The most important such contribution at 33°K arises from the transition $\Gamma_4 \rightarrow \Gamma_5(+)$, which ought to coincide closely with (1-6). If we assume that this line is sufficiently broad at 33°K to contribute more or less equally to the measured intensity assigned to the transitions (1-6) and (2-6) [the line (1-7) is too broad to be observed at $T > 35$°K], then the principal effect of including these additional transitions is to diminish the predicted relative intensities of lines (3-6), (4-6), and (5-6) in Table XIII by about one-quarter.

[89] The value $\rho \approx -K$ together with the strong quenching of ζ would be consistent with a microscopic model in which the principal Jahn-Teller coupling is with an E vibrational mode. However, this model would predict that μ should then be reduced, like ζ, to a small fraction of its crystal field value. The much larger value found for μ indicates that the correct model must be more complicated, probably because T_2 modes play an important role even though an E mode may couple most strongly.

trum, unless our identification of some of the lines is in error. In particular, if the line (1-8) is not the $\Gamma_1 \rightarrow \Gamma_4(+)$ transition, but instead perhaps a line belonging to Fe^{2+} associated with some defect, then other choices for the parameters become possible. Alternatively, if (1-8) is a $\Gamma_1 \rightarrow \Gamma_5$ transition appearing because a third Γ_5 vibronic state has been depressed in energy by the Jahn-Teller coupling, the Hamiltonian in Eq. (4.3) will not suffice. These alternative possibilities cannot be ruled out on the basis of the present data.

Fe^{2+} in $MgAl_2O_4$

The spectrum of Fe^{2+} in $MgAl_2O_4$ at 6.9°K has two strong zero-phonon lines, (1-6) and (1-7), separated by 65 cm^{-1}, which we ascribe to the electric-dipole allowed transitions $\Gamma_1 \rightarrow \Gamma_5(\pm)$ from level No. 1. Assuming that the Hamiltonian (4.3) may be used, we find from this separation between levels $\Gamma_5(-)$ and $\Gamma_5(+)$, using Eq. (4.30), that we may place bounds on the values for $|\zeta-\mu|$ which can be consistent with the spectrum, namely

$$|\zeta-\mu| = 13 \pm 2 \text{ cm}^{-1}. \tag{5.11}$$

In obtaining this result, we have used the fact that the oscillator strengths of (1-6) and (1-7) are comparable, and that consequently we must have $|x| \lesssim \frac{1}{2}$ for the parameter (4.28).

There is insufficient additional information in the observed spectrum in this case to permit a unique determination of the parameters ζ, μ, and ρ. As the temperature is raised, lines (2-6), (3-6), and (4-6) appear, as expected from Table XI, spaced uniformly on the low-energy side of (1-6) with a separation 13 ± 2 cm^{-1}, and a line (2-7) appears separated from (1-7) by approximately the same interval. No further lines are resolved which we can ascribe to transitions to other levels of $^5T_2$ from levels No. 2 through No. 5. However, (1-7) and (2-7) are quite broad and could easily obscure additional lines in this part of the spectrum, while such transitions occurring at higher frequency than (1-7) may be too broad to be resolved. We can conclude from these results that the other levels of $^5T_2$ are almost certainly higher in energy than $\Gamma_5(-)$, but we cannot determine their positions more definitely. There is accordingly a fairly broad range of possible choices for ζ, μ, and ρ which are compatible with the observed spectrum, in particular with (5.11), and also with the assumption that ζ is positive and larger than it is for Fe^{2+} in ZnS [since Q in (5.8) is not so small for $MgAl_2O_4$ as for ZnS]. In view of these uncertainties, we have not attempted to identify the weak line (1-8) which appears at 6.9°K at higher frequency than (1-7). This line may be a transition from level No. 1 to one of the other levels of $^5T_2$, made weakly allowed by strain, or like other lines at higher frequency it may be a transition to a higher vibronic state not described by the phenomenological Hamiltonian (4.3).

Fe^{2+} in CdTe

The spectrum of Fe^{2+} in CdTe at 3.5°K shows three strong zero-phonon lines (1-6), (1-7), and (1-8) within a range of only ≈ 30 cm^{-1}. These presumably are $\Gamma_1 \rightarrow \Gamma_5$ transitions from level No. 1. As we have noted earlier, more than two Γ_5 levels cannot be reconciled with the Hamiltonian (4.3). We would therefore need a more complicated phenomenological Hamiltonian to describe $^5T_2$ for this case, in all likelihood because other vibronic states have been depressed in energy by the Jahn-Teller coupling.

As the temperature is raised, the three additional lines (2-6), (3-6), and (4-6) appear on the low-frequency side of (1-6). Together with (1-6) these lines make up a group of four more or less evenly spaced lines (interval 10 ± 2 cm^{-1}) which we ascribe to transitions from levels No. 1 through No. 4 of ^5E to the lowest Γ_5 level of $^5T_2$. The corresponding transition from level No. 5 (Γ_2) is electric-dipole forbidden, and no line corresponding to this transition has been observed. This lowest Γ_5 level is evidently the lowest level of $^5T_2$, as there are no additional lines at lower frequency than (1-6) which could be ascribed to other transitions from levels No. 2–No. 5. The transition from level No. 2 to the second Γ_5 level should give a line very nearly coinciding with (1-6), and indeed (1-6) seems to gain in relative intensity as the temperature rises (Fig. 7). Other lines that should appear with increasing temperature may well be obscured by (1-6), (1-7), and (1-8).

We have not attempted to fit this spectrum to a more general Hamiltonian than (4.3) because we have at present insufficient data to determine the necessary generalization. Accordingly, we have not tried to identify the weak lines (1-9) and (1-10) or to infer a value for the spin-orbit quenching factor for this case.

E. Alternative Model for Fe^{2+} in ZnS

An alternative interpretation of the spectrum of Fe^{2+} in ZnS may be proposed if it is assumed that the two weak zero-phonon lines (1-7) and (1-8) (Table II and Figs. 2, 3, 4) do not belong to the spectrum of an isolated Fe^{2+} ion in tetrahedral symmetry. These lines appeared in the spectra of all the samples that were studied at the low temperatures (R139, R118, and R114A), and despite the differences in the history and iron concentration of these samples (Table I) the lines had in all cases the same oscillator strength (to within an experimental uncertainty of $\pm 50\%$). Nevertheless, despite such evidence that these lines belong to the same center that gives rise to the rest of the spectrum, it is possible that they arise from Fe^{2+} associated with some other defect in the ZnS, or that they arise from small regions of hexagonal ZnS included in the predominantly cubic crystals. The presence of such regions having an hexagonal structure and representing 1% to 20% of the volume of some natural crystals of cubic ZnS has been suggested by Smith[90] from x-ray data.

[90] F. G. Smith, Am. Mineral. **40**, 658 (1955).

The content of various metallic impurities in the ZnS crystals used in the present study has been measured and is given in Table I. The possible content of oxygen, which substitutes for sulfur, has been estimated from the measured lattice constant.[91] For this estimate the measured lattice constants in Table I were slightly reduced in order to account for the presence of the Fe, Cd, and Mn impurities.[92] The oxygen content is $<3\times10^{19}$ atoms/cm^3 if the lattice constant of pure ZnS is taken as 5.4093 Å at 300°K. Skinner and Barton[91] believe that natural ZnS crystals contain much less oxygen than this upper limit. The wide range observed in the concentration of trace impurities other than Fe coupled with the fact that the absorption lines (1-7) and (1-8) are present at very nearly the same oscillator strength in all three crystals studied, makes us believe that these two lines are not associated with impurity effects. The two lines labeled EX in Figs. 4 and 5 appear to be associated with Fe-Fe interactions.

In order to determine whether there were significant volumes of hexagonal ZnS inclusions in the natural crystals, thin, polished sections were analyzed under a microscope using crossed polarizers. Any hexagonal inclusions, if present in regions of 100 μ or larger in size, occupied less than 1% of the crystal volume. In order to eliminate the possibility that the crystals possessed hexagonal inclusions on a submicroscopic scale W. Roth of this laboratory kindly took single-crystal rotation and precession x-ray photographs of [111] axis rods from samples R114 and R118. He found no evidence of hexagonal regions, and concluded that any hexagonal regions present constituted less than 3% of the crystal volume. The absorption spectrum of a synthetic, Fe-doped hexagonal ZnS crystal has also been measured at 4°K. It showed two different (1-6) transitions, one at 2950 cm^{-1} similar to cubic ZnS and a second one at 2829 cm^{-1} weaker by a factor of 8. There were no pronounced lines near the cubic (1-7) and (1-8) transitions. Thus the possibility that lines (1-7) and (1-8) are caused by Fe^{2+} ions in a hexagonal crystal environment is believed to be remote. It seems reasonable therefore to conclude that lines (1-7) and (1-8) are caused by the same Fe^{2+} ions that cause line (1-6); however, we cannot at this time altogether rule out the following alternative model.

Omitting lines (1-7) and (1-8) from the spectrum to be explained, we may try to account for the rest of the spectrum on the basis of a model for the $^5T_2$ state which accords more nearly with the predictions of crystal-field theory and which does not require a strong Jahn-Teller effect. In this model, we would ascribe line (1-6) to the electric-dipole transition to the $J'=1$ triplet level (Γ_5) of $^5T_2$ [(4.7) and Fig. 10]. Lines (2-6), (3-6), and (4-6) should then appear as the crystal is warmed, with oscillator strengths relative to that of (1-6) as given by Table X. For $T=33$°K we find in fact from Table X that the relative integrated intensity of lines (1-6), (2-6), (3-6), and (4-6) should be 1.00, 1.18, 0.28, and 0.10, respectively, on this model, in not bad agreement with the observed values given in Table XIII. Line (5-6), however, should be weaker on this model than it is observed to be (Table XIII), since the transition $\Gamma_2\rightarrow\Gamma_5$ is electric-dipole forbidden. The ratio of intensities of (5-6) and (1-6) at 33°K should be no larger than 1×10^{-4} [93] if (5-6) arises from a magnetic-dipole process, whereas the observed ratio is 1×10^{-2}. However, (5-6) may perhaps "borrow" additional intensity from the strong electric-dipole lines because of the effect of strains at some of the Fe^{2+} sites.

On the basis of this alternative model, a second strong zero-phonon line corresponding to the transition from Γ_1 of ^5E to the $J'=3$, Γ_5 level would be expected to appear among the phonon-assisted lines associated with transitions from Γ_1 to $J'=1$, while at temperatures at which levels Nos. 2–5 are populated zero-phonon lines from these levels to both $J'=2$ and 3 should appear with $\bar{\nu}>3000$ cm^{-1}. Although the lines with $\bar{\nu}>3000$ cm^{-1} have been identified as phonon-assisted transitions in Table IV and Fig. 3, such an alternative identification of certain of these lines remains a possibility.

When account is taken of interaction of the Fe^{2+} with phonons, this alternative model leads to the same assignment of phonon energies as given in Table V, if the phonon-assisted peaks labeled in Fig. 3 are associated with the electronic transition to the $J'=1$ level. Use of this model also does not change our determination (5.1) of Dq from the moment ratio (4.21), nor the value obtained for a^2 in (5.2). If this model is correct the value (5.5) is of course much too large for the true Jahn-Teller energy, and the reduction factor Q in (5.8) much too small. While the $J'=1$ level still lies 535 cm^{-1} below the position of $\bar{E}(^5T_2)$ given by Eq. (4.22), this energy difference must arise in this model principally from the spin-orbit splitting of $^5T_2$ and from coupling to symmetric modes of vibration. Only a very small part of this energy difference can now be a true Jahn-Teller energy, since if the Jahn-Teller splitting of $^5T_2$ is smaller than the spin-orbit splitting, then as Van Vleck and Liehr[94] have shown the spin-orbit interaction largely suppresses all Jahn-Teller effects in the $J'=1$ level.

VI. DISCUSSION AND CONCLUSIONS

While crystal-field theory accounts well for the observed splitting of the ^5E ground state of tetrahedral Fe^{2+} in ZnS, CdTe, and $MgAl_2O_4$ (see Table III),

[91] B. J. Skinner and P. B. Barton, Am. Mineral. **45**, 612 (1960).
[92] B. J. Skinner, Am. Mineral. **46**, 1399 (1961).

[93] This value is obtained from Table X by taking for b^2/a^2 the ratio of the free-ion value $b^2=4.2\times10^{-6}(\varepsilon/\varepsilon_{\text{eff}})^2$ (Sec. IVA) to the value $a^2=6.4\times10^{-4}$ obtained in Table VI from the integrated intensity of the entire $^5E\rightarrow{}^5T_2$ band.
[94] J. H. Van Vleck, Physica **26**, 544 (1960); Discussions Faraday Soc. **26**, 98 (1958); A. D. Liehr, Bell System Tech. J. **39**, 1617 (1960).

TABLE XIV. Summary of the parameters derived from optical absorption studies of the ${}^5E \rightarrow {}^5T_2$ band of tetrahedral Fe^{2+}.

Parameter[a]	Units	Host crystal ZnS	CdTe	$MgAl_2O_4$
Dq	cm^{-1}	-340	-248	-447
K	cm^{-1}	$+15\pm2$	$+10\pm2$	$+13\pm2$
λ^2/Δ	cm^{-1}	$+2.5\pm0.3$	$+1.7\pm0.3$	$+2.2\pm0.3$
$\lvert\lambda\rvert$	cm^{-1}	92 ± 10	64 ± 10	98 ± 10
a^2	10^{-4}	6.4	1.8	5.0
$E_{JT}({}^5T_2)$	cm^{-1}	535	255	945
$(F_0/F_{tot})_{0°K}$	...	0.08	0.16	0.15
$E_{JT}({}^5T_2)/\langle\hbar\omega\rangle$[b]	...	2.5	1.8	1.9
$\langle\hbar\omega\rangle$	cm^{-1}	215	140	495
Q(l.b.)	...	0.023	0.06	0.06
ζ	cm^{-1}	$+3.0$[c]	...	...
μ	cm^{-1}	$+4.5$[c]	...	...
ρ	cm^{-1}	-14.0[c]	...	...
x		-0.90[c]	...	$\lvert x\rvert \lesssim \frac{1}{2}$[d]
y		-0.85[c]	...	...
$\lvert\zeta-\mu\rvert$	cm^{-1}	...	...	13 ± 2[d]
TA	cm^{-1}	115 ± 5	65 ± 3	...
LA	cm^{-1}	184 ± 4	105 ± 3	...
TO	cm^{-1}	296 ± 3	140 ± 3	...
LO	cm^{-1}	331 ± 3	180 ± 3	...

[a] The identification of the tabulated parameters is as follows (the indicated reference is to the equation in the text where the tabulated values were obtained): Dq is the one electron cubic crystal-field parameter [(5.1)]; K is the splitting parameter of the ${}^5E$ ground term, as defined by (4.1) [(5.3)]; λ^2/Δ is the second-order spin-orbit parameter resulting from the spin-orbit coupling between ${}^5E$ and ${}^5T_2$ [obtained from the value for K, using Eq. (4.2), on the assumption that Jahn-Teller effects in ${}^5E$ are negligible]; λ is the parameter specifying the Fe^{2+} spin-orbit interaction $\lambda(\mathbf{L}\cdot\mathbf{S})$ within the electronic states derived from ${}^5D$ (obtained from λ^2/Δ using $\Delta = 10|Dq|$) [(5.4)]; a^2 is the parameter giving the total oscillator strength at 0°K for the ${}^5E \rightarrow {}^5T_2$ absorption band [see Eqs. (4.15) and (4.19)] on the basis of an electric-dipole–allowed process [(5.2)]; $E_{JT}({}^5T_2)$ is the Jahn-Teller energy of the ${}^5T_2$ state [(5.5)]; $(F_0/F_{tot})_{0°K}$ is the fraction of the total oscillator strength of the full ${}^5E \rightarrow {}^5T_2$ band at 0°K which is contributed by the zero-phonon transitions [Table VI]; $\langle\hbar\omega\rangle$ is the average energy of the phonons effective in the Jahn-Teller coupling (averaged in the sense of Ref. 85) [(5.7)]; Q(l.b.) is the lower bound (5.8) for the Jahn-Teller quenching factor Q for spin-orbit interaction, given by Eq. (4.23); ζ, μ, ρ are the parameters of the Hamiltonian (4.3) used to describe the lowest vibronic levels of ${}^5T_2$ for ZnS and $MgAl_2O_4$ [(5.9)]; x, y are the parameters defined by Eqs. (4.28)–(4.29) which give the relative oscillator strengths of the zero-phonon lines obtained with the Hamiltonian (4.3) [(5.10)]; TA, LA, TO, LO are the energies of the various lattice phonons of the host crystal [Tables V and VII].

[b] From (5.6).

[c] From (5.9) and (5.10).

[d] From (5.11) and related text.

we have seen that it fails to provide a satisfactory description of the levels of the excited state, ${}^5T_2$ [unless possibly, for Fe^{2+} in ZnS, the zero-phonon lines (1-7) and (1-8) are not really part of the spectrum of tetrahedral Fe^{2+}, in which case the alternative model may provide a description of this spectrum not in disagreement with crystal-field theory]. We have therefore supplemented crystal field theory by assuming that in tetrahedral symmetry a pronounced dynamical Jahn-Teller effect occurs in ${}^5T_2$, and we have shown that this assumption is consistent with the relative intensity of the zero-phonon and phonon-assisted parts of the low-temperature spectra. We have seen that despite the Jahn-Teller coupling it may still be possible to find a phenomenological Hamiltonian which describes the lowest levels of ${}^5T_2$, but that the parameters in this Hamiltonian (and possibly also its form) may be quite different from those given by crystal-field theory. We have found that such a Hamiltonian does account quite satisfactorily for the observed zero-phonon spectrum of Fe^{2+} in ZnS, and we have obtained the parameters explicitly. A Hamiltonian of the same form was found to be consistent too with the spectrum of Fe^{2+} in $MgAl_2O_4$; however all of the parameters could not be determined uniquely for this case. For Fe^{2+} in CdTe, on the other hand, a more general form for the phenomenological Hamiltonian was shown to be required, but the data did not suffice to determine an explicit result. In all three cases, despite the differences in detail, the strengths of the Jahn-Teller coupling in ${}^5T_2$ were found to be comparable and were sufficient to quench the first-order spin-orbit splitting to a small fraction of its crystal-field value. Values obtained from these spectra for the various parameters characterizing the levels of Fe^{2+} in each crystal are summarized in Table XIV.

We are not able at present to give a microscopic model of the dynamical Jahn-Teller effect for Fe^{2+} in these crystals, on the basis of which we could derive the parameters of the phenomenological Hamiltonian for ${}^5T_2$ from the properties of the Fe^{2+} ion and the appropriate values of the electron-lattice coupling parameters. On the one hand the proper values for such coupling parameters in these crystals are not known, and on the other hand the mathematical theory of the dynamical Jahn-Teller effect for an orbital triplet is very complicated and has not been worked out for a realistic case. The form of the phenomenological Hamiltonian obtained for Fe^{2+} in ZnS suggests that the dominant Jahn-Teller coupling in this case may be with an E vibrational mode, while the appearance of a third Γ_5 level among the lowest levels of ${}^5T_2$ for Fe^{2+} in CdTe suggests that a T_2 mode may dominate in this case. Unfortunately, the dynamical Jahn-Teller effect is still too imperfectly understood in realistic situations to permit definite conclusions to be drawn at this time concerning the basic mechanisms involved in each case. We must remember, of course, that such agreement as has been obtained with the phenomenological Hamiltonian may be fortuitous; the correct description of the vibronic levels derived from ${}^5T_2$ may be very much more complicated. Such complications are certain to be present [and the use of a simple Hamiltonian like (4.3) impossible] when the Jahn-Teller splitting ($\approx 3E_{JT}$), the spin-orbit splitting ($\approx 5\lambda$) and the phonon energies are all of the same size. For Fe^{2+} in the crystals considered here, the values we obtain for the Jahn-Teller splitting are larger than those for spin-orbit splitting and the phonon energies, but not by too great a margin.

Alternatively, in the case of Fe^{2+} in ZnS, we have seen that a more conventional interpretation of the spectrum may be possible if two of the weak zero-phonon lines are assumed to arise from some other center. On this model Jahn-Teller effects appear to play no prominent role for Fe^{2+} in ZnS, at least as far as the lowest energy group of zero-phonon transitions to ${}^5T_2$ are concerned. It should be noted, however, that a similar interpretation of the spectra of Fe^{2+} in CdTe and $MgAl_2O_4$ would not appear to be possible, since the additional

zero-phonon lines not accounted for by the crystal-field model in these spectra have intensity comparable to that of (1-6). Accordingly a moderately strong dynamical Jahn-Teller effect as proposed in this paper evidently *is* required in these crystals (whether or not a simple phenomonological Hamiltonian is useful) in order to effect so large a reduction in the spin-orbit splitting of $^5T_2$ and to bring down additional states originating in higher vibrational levels. This being so for CdTe and $MgAl_2O_4$, it would appear likely that Jahn-Teller effects should also be of importance for the $^5T_2$ state in ZnS. For this reason as well as others we have noted, we favor the interpretation of all three spectra as showing pronounced Jahn-Teller effects.

Further verification of our identification of the various zero-phonon lines in the spectra would be desirable, for example by studying the splitting of these lines under an applied stress as done by Sturge[95] in his investigation of Jahn-Teller effects in the $^4T_{2g}$ excited state of V^{2+} in MgO. Such experiments have not been attempted for the crystals we have studied; they would be particularly useful because they would also yield values for the electron-lattice coupling parameters, which are needed both to test our estimates of the Jahn-Teller energy and of the contribution of symmetric modes to the broadening of the absorption band, and to aid in the construction of a microscopic model for the Jahn-Teller effects.

From the structure in the phonon-assisted portion of these spectra, we have been able to infer values for the energies of the maxima in the effective density of states of the phonons with which the Fe^{2+} ion interacts. The four energies obtained for these maxima from the spectrum of Fe^{2+} in ZnS (Table V) agree quite well with values that have been obtained by other methods for the energies of the unperturbed lattice phonons TA, LA, TO, and LO of pure ZnS at the Brillouin zone edge. Since the mass and ionic radius of the Fe^{2+} ion are not very different from those of the Zn^{2+} ion that the Fe^{2+} replaces, it is reasonable that the phonon energies should be characteristic of the host lattice rather than of distinct local modes of vibration of Fe^{2+} and its near neighbors. For Fe^{2+} in CdTe, however, we can be less confident that the four phonon energies obtained from the spectra and given in Table VII represent unperturbed lattice phonons, since the Fe^{2+} ion is appreciably both lighter and smaller than Cd^{2+}. Nevertheless, published values for the energies of the TO and LO phonons in pure CdTe agree reasonably well with the two larger values which we obtain. We assume therefore that our two smaller values give approximate energies for the TA and LA phonons of CdTe, for which no previous data exist. Finally, for $MgAl_2O_4$ we have made no attempt to identify the phonon energies obtained (Table VIII), because of the complex crystal structure, the difference in mass between Mg^{2+} and Fe^{2+}, and the lack of previous data on the phonon spectrum. Nevertheless, it is evident from Table VIII that similarities exist between the phonon energies we obtain and the peaks observed in the reflectivity of the host crystal in the infrared. For none of these crystals have we attempted an interpretation of the intensities of the individual phonon-assisted lines. The relative intensities of these lines should provide data relating to the microscopic model of the Jahn-Teller effects and the nature of the electron-lattice coupling; however we have deferred an attempt to exploit this information until our understanding of the basic mechanisms of the Jahn-Teller effects shall have improved.

[95] M. D. Sturge, Phys. Rev. **140** A880 (1965).